An Analysis of AERONET Aerosol Absorption Properties and Classifications Representative of Aerosol Source Regions

D. M. Giles,[1,2,3] B. N. Holben,[2] T. F. Eck,[2,4] A. Sinyuk,[1,2] A. Smirnov,[1,2] I. Slutsker,[1,2] R. R. Dickerson,[3] A. M. Thompson,[5] and J. S. Schafer[1,2]

1. Sigma Space Corporation, Lanham, MD 20706 USA
2. Biospheric Sciences Laboratory, NASA Goddard Space Flight Center, Greenbelt, MD 20771 USA
3. Department of Atmospheric and Oceanic Science, The University of Maryland, College Park, MD 20742 USA
4. Universities Space Research Association, Columbia, MD 21044 USA
5. Department of Meteorology, The Pennsylvania State University, University Park, PA 16802 USA

Submitted to the Journal of Geophysical Research–Atmospheres

AGU Index Terms: 0305, 0345, 0360

Abstract

Partitioning of mineral dust, pollution, smoke, and mixtures using remote sensing techniques can help improve accuracy of satellite retrievals and assessments of the aerosol radiative impact on climate. Spectral aerosol optical depth (τ) and single scattering albedo (ω_o) from Aerosol Robotic Network (AERONET) measurements are used to form absorption [i.e., ω_o and absorption Ångström exponent (α_{abs})] and size [i.e., extinction Ångström exponent (α_{ext}) and fine mode fraction of τ] relationships to infer dominant aerosol types. Using the long-term AERONET data set (1999-2010), 19 sites are grouped by aerosol type based on known source regions to: (1) determine the average ω_o and α_{abs} at each site (expanding upon previous work); (2) perform a sensitivity study on α_{abs} by varying the spectral ω_o; and (3) test the ability of each absorption and size relationship to distinguish aerosol types. The spectral ω_o averages indicate slightly more aerosol absorption (i.e., a $0.0<\delta\omega_o\leq0.02$ decrease) than in previous work and optical mixtures of pollution and smoke with dust show stronger absorption than dust alone. Frequency distributions of α_{abs} show significant overlap among aerosol type categories and at least 10% of the α_{abs} retrievals in each category are below 1.0. Perturbing the spectral ω_o by ±0.03 induces significant α_{abs} changes from the unperturbed value by at least $\sim\pm0.6$ for Dust, $\sim\pm0.2$ for Mixed, and $\sim\pm0.1$ for Urban/Industrial and Biomass Burning. The ω_{o440nm} and $\alpha_{ext440\text{-}870nm}$ relationship shows the best separation among aerosol type clusters, providing a simple technique for determining aerosol type from surface- and future space-based instrumentation.

1.0 Introduction

Particles suspended in the atmosphere are difficult to characterize both temporally and spatially due to their short lifetime and geographically diverse sources. Aerosol mixtures—whether dominated by dust, sulfate, carbon, sea salt, or mixtures of these particles—pose a challenge to satellite and sub-orbital remote sensing techniques when identifying aerosol type [*Jeong and Li* 2005; *Levy et al*., 2007; *Kalapureddy et al*., 2009; *Lee et al*., 2010; *Kahn et al*., 2010; *Russell et al*., 2010]. Remote sensing techniques can quantify the aerosol particle size using spectral aerosol optical properties, but inferring aerosol type requires knowledge of the source regions usually obtained through use of ancillary data sets (e.g., back trajectory models, satellite product, electron microscopy) to determine emission sources, transport mechanisms, composition, and morphology. The discrimination of aerosol types increases accuracy of the assessment of the aerosol radiative impact and therefore is important to climate modeling [*Diner et al*., 1999; *Satheesh and Moorthy* 2005]. Variations in spectral aerosol absorption magnitudes can enable partitioning among aerosols from various source regions, fuel types, or combustion phases. Aerosol absorption together with size can potentially determine dominant aerosol type from remote sensing and in situ measurements.

Various methods have been proposed using aerosol optical and microphysical properties to distinguish aerosol types. The magnitude of the aerosol optical depth (AOD, τ_{ext}) and the spectral dependence of AOD with respect to wavelength (i.e., Ångström exponent, α_{ext}) is commonly used in aerosol remote sensing to infer dominant aerosol types given knowledge of the source region or typical aerosol transport mechanisms [e.g., *Kalapureddy et al.*, 2009, *Boselli et al*., 2012]. Other techniques using the derivative of the Ångström exponent or spectral difference of Ångström exponent wavelength pairs along with aerosol loading and particle

effective radius may provide further information on particle type with respect to size and growth of particles [*Gobbi et al*., 2007; *Basart et al.,* 2009]. Although size varies among particle types, the spectral absorption also varies. Studies [*Omar et al*., 2005, *Levy et al*., 2007; *Mielonen et al*., 2009; *Lee et al*., 2010; *Russell et al*., 2010] have suggested relationships utilizing the aerosol absorption and size properties to determine the dominant aerosol type from Aerosol Robotic Network (AERONET) retrievals [*Holben et al*., 1998; *Dubovik et al*., 2000; *Dubovik et al*., 2002; *Dubovik et al*., 2006]. Information content from these relationships varies from generic identification of major aerosol particle types (e.g., dust, mixed, urban/industrial pollution, and biomass burning smoke) to specific degrees of absorbing aerosols. Recently, *Russell et al.* [2010] have proposed using the absorption Ångström exponent (AAE, α_{abs}), the spectral absorption aerosol optical depth dependence on wavelength, to further define aerosol type from AERONET retrievals. For comparison to the Cloud-Aerosol Lidar with Orthogonal Polarization (CALIOP) instrument, *Mielonen et al.* [2009] utilized the AERONET single scattering albedo (ω_o) difference between 440 and 1020 nm (as suggested by *Bergstrom et al.* [2002] and implemented by *Derimian et al.* [2008]) and α_{ext} to estimate aerosol type. Further, *Lee et al.* [2010] modified this relationship to use only ω_o from 440 nm and the fine mode fraction (η) of the AOD at 550 nm to determine the particle size partitioning. Other techniques using spectral lidar ratios and multiple aerosol optical and microphysical properties retrieved from AERONET have been implemented to determine aerosol type categories for various applications [*Cattrall et al*., 2005; *Omar et al*., 2005; *Qin and Mitchell* 2009; *Burton et al*., 2012].

In this study, for data available between 1999 and 2010, 19 AERONET sites were classified by dominant aerosol type [i.e., Dust, Mixed, Urban/Industrial (U/I), and Biomass Burning (BB)] based on previous literature. First, aerosol absorption parameters (i.e., ω_o and

α_{abs}) were analyzed and compared to previous work. Second, sensitivity tests were performed on the α_{abs} by perturbing ω_o to determine variability within each dominant aerosol type category. Last, the absorption and size relationships were evaluated and compared to each other based on the dominant aerosol type categorizations.

2.0 Instrumentation and Method

The Aerosol Robotic Network is a ground-based network of standardized Cimel Sun and sky scanning radiometers measuring AOD at multiple wavelengths from 340 to 1640 nm and retrieving other columnar optically effective aerosol properties (e.g., volume size distribution, complex index of refraction, and single scattering albedo) from sky radiance measurements at four wavelengths: 440, 675, 870, and 1020 nm [*Holben et al*., 1998]. The AOD estimated uncertainty varies spectrally from ±0.01 to ±0.02 with the highest error in the ultraviolet wavelengths [*Holben et al*., 1998; *Eck et al*., 1999] and calibrated sky radiance measurements typically have an uncertainty less than 5% [*Holben et al*., 1998]. Further descriptions of the instrumentation, calibration, methodology, data processing, and data quality are described elsewhere [*Holben et al*., 1998; 2006; *Eck et al*., 1999; 2005; *Smirnov et al*., 2000]. For all sky radiance wavelengths (440, 675, 870, and 1020 nm), the ω_o uncertainty is expected to be ±0.03 based on Version 1 almucantar retrieval computations when τ_{440nm}>0.4 [*Holben et al.*, 1998; *Eck et al*., 1999; *Dubovik et al*., 2002]. When compared to AERONET ω_o retrievals, in situ measurements of ω_o were within AERONET uncertainty estimates [*Leahy et al*., 2007; *Johnson et al*., 2009; *Müller et al*., 2010; *Toledano et al*., 2011].

In-depth discussions of the almucantar retrieval products are given by *Dubovik and King* [2000] and *Dubovik et al.* [2000; 2002; 2006] and quality criteria are discussed by *Holben et al.*

[2006]. *Dubovik et al.* [2002] provided averaged almucantar retrieval aerosol optical and microphysical properties based on aerosol types and source region using AERONET pre-Version 1 data (i.e., data collected and analyzed prior to the release of quality assured Version 1 retrieval data set in 2003). These results have been used throughout the literature to define aerosol type based on the aerosol absorption characteristics [*Russell et al*., 2010 and references therein]. Notably, the Version 2 retrievals (i.e., released in 2006) utilized new input data sets (e.g., NCEP reanalysis, MODIS ecosystem type-based BRDF functions, and geographically and temporally varying black sky albedo), more dynamic calculations of the surface reflectance than the Version 1 assumption of a green Earth surface reflectance, robust quality checks of the measured sky radiance inputs, and improved criteria for acceptable sky residual fits [*Holben et al.*, 2006; *Leahy et al.*, 2007; *Eck et al.*, 2008 and references therein]. For example, in the United Arab Emirates and Arabian Gulf, Version 2 improvements provided more consistent ω_o magnitudes and spectra for coarse-mode dust aerosol over two vastly different surfaces (i.e., small island versus bright desert) with ω_o differences of less than 0.01 compared to 0.03 for the Version 1 spheroid inversion model and with increased absorption at 440 nm, which typically occurs in iron-rich desert dust, rather than spectrally neutral ω_o from Version 1 retrievals [*Eck et al.*, 2008].

Additional instrument checks were implemented to assess absorption properties from the Version 2 almucantar retrievals. To improve the quality of the sky radiance measurements used for almucantar retrievals, instrument collimator consistency checks were performed to remove potential artifacts (e.g., induced by spider webs in the tube, excessive dust, or contamination on the sensor head window due to moisture or dust) in the radiance measurements. The sky radiance measurements at ±6° azimuth from solar zenith—using the solar aureole and sky gains for instruments with only Silicon detectors—were required to have a percent difference of less

than 10% spectrally from 440 to 1020 nm. For Silicon and InGaAs detector instruments (where each detector measures in a different collimator tube), the temperature corrected Silicon and InGaAs $\tau_{1020\ nm}$ difference ($\Delta\tau$) must be less than $\Delta\tau_{limit}$ of 0.06/*m* (where *m* is the optical air mass), which results in a $\Delta\tau_{limit}$ of 0.03 when *m* equals 2 and 0.06 for the overhead sun (*m*=1). Collimator consistency checks provide an improved method to further quality assure the Level 2.0 almucantar retrieval data set.

Measured aerosol optical depth and computed almucantar retrieval products can be used to derive additional aerosol properties. The extinction Ångström exponent (α_{ext}) was calculated from the spectral dependence of AOD or τ_{ext} with wavelength (λ) using equation (1) [*Ångström* 1964]:

$$\alpha_{ext} = -d\ln[\tau_{ext}(\lambda)]/d\ln(\lambda) \quad (1)$$

For a wavelength range between 440 and 870 nm typically using 440, 500, 675, and 870 nm AOD—and computed by linear regression of ln τ versus ln λ—values near 0 indicate mainly coarse mode (radius, r>1 μm) aerosol particles, while values near 2 indicate mainly fine or accumulation mode (r<1 μm) aerosol particles [*Holben et al*., 1991; *Kaufman et al*., 1992; *Eck et al*., 1999; *Reid et al*., 1999; *Holben et al*., 2001]. The absorption AOD or τ_{abs} is calculated for each wavelength using equation (2):

$$\tau_{abs}(\lambda) = \tau_{ext}(\lambda) * [1-\omega_o(\lambda)] \quad (2)$$

[*Eck et al*., 2010; *Russell et al*., 2010; *Giles et al*., 2011a]. Similar to α_{ext}, the spectral dependence of τ_{abs} with λ on logarithmic scale gives the absorption Ångström exponent or α_{abs} in equation (3):

$$\alpha_{abs} = -d\ln[\tau_{abs}(\lambda)]/d\ln(\lambda) \quad (3)$$

Assuming a spectrally constant index of refraction, very small spherical black carbon particles (r ~0.01 μm) can have a λ^{-1} dependence or α_{abs} of 1.0 [*Bergstrom et al*., 2002], while larger optically effective black carbon particles (e.g., r>0.1 μm) may have α_{abs} values below 1.0 for large cores and up to 1.6 for various shell coatings [*Lack and Cappa* 2010]. *Russell et al.* [2010] analyzed AERONET pre-Version 1 almucantar retrievals from *Dubovik et al.* [2002] and showed α_{abs} values vary between ~1.2 and 3.0 for Dust, ~0.75 and 1.3 for U/I, and ~1.2 and 2.0 for BB. *Eck et al.* [2010] analyzed AERONET Version 2 almucantar retrievals and showed sites dominated by optical mixtures of dust, smoke, and pollution had α_{abs} values between ~1.2 and 1.8 for mixed size particles (i.e., fine mode fraction of the AOD at 675 nm ranged between ~0.35 and 0.65). In the present study, the fine mode AOD (τ_f) and coarse mode AOD (τ_c) from the almucantar retrieval—as inferred from the size distribution and refractive indices—were interpolated to 550 nm using the linear fit of the logarithms of τ_f, τ (i.e., $\tau_f+\tau_c$) for 440, 675, and 870 nm wavelengths to calculate the fine mode fraction of the AOD [i.e., $\eta = \tau_f/(\tau_f+\tau_c)$] at 550 nm ($\eta_{550nm}$).

Nineteen AERONET sites were selected for the analysis based on the availability of an extensive data record (i.e., greater than five data equivalent years of AOD measurements from 1999 to 2010) and the geographic distribution among aerosol source regions (Figure 1). The sites were designated as one of four commonly used aerosol classifications: Dust, Mixed, Urban/Industrial (U/I), and Biomass Burning (BB). The classifications were established based on the source regions and known seasonal changes in aerosol type over these regions (see references in Table 1). Further, these selected sites should be subject to high aerosol loading (i.e., τ_{440nm}>0.4) to meet the Version 2, Level 2.0 almucantar retrieval sensitivity requirement for absorption parameters (e.g., ω_o, τ_{abs}) [*Dubovik et al*., 2000; *Holben et al*., 2006]. Sea salt (as well

as biogenic) aerosols as a dominant particle type category were not considered in this study since τ_{500nm} is typically less than 0.1 for pure maritime environments [*Smirnov et al*., 2002]; however, for maritime locations affected by aerosol plumes (e.g., Saharan dust transport over Cape Verde islands), $\tau_{440nm}>0.4$ can be satisfied [*Smirnov et al*., 2009]. Hence, the $\tau_{440nm}>0.4$ criterion biases the data set only to high aerosol loading periods to ensure enough radiometric sensitivity to compute absorption reliably [*Dubovik et al*., 2002]. Although Dust, U/I, and BB categories may represent the dominant aerosol type, episodic aerosol incursions outside of their classification category likely have occurred at any site during the analysis period (e.g., dust over Shirahama or Lake_Argyle, biomass burning smoke over GSFC) [*Sano et al*., 2003; *Qin and Mitchell* 2009; *Eck et al.*, 2003b; *O'Neill et al.*, 2005]. The Mixed aerosol category encompasses sites primarily affected by different mixtures of aerosol types (e.g., dust and pollution or dust and biomass burning smoke mixtures) on a seasonal basis, increasing the probability of at least an optical mixture state [*Derimian et al.*, 2006; *Eck et al.*, 2010]. Although no explicit seasonal partitioning is performed, the $\tau_{440nm}>0.4$ criterion captures mainly seasonal increases in aerosol loading at some sites (e.g., GSFC and Mongu) [*Holben et al.*, 2001].

3.0 Results

3.1 Retrieved Absorption Properties by Dominant Aerosol Type

Dust particles aggregated with varying combinations of clay, quartz, and hematite exhibit strong absorption in the blue wavelength region (e.g., 440 nm) with lower absorption in the visible and near infrared wavelengths (i.e., ω_o increasing with wavelength) [*Sokolik and Toon* 1999]. For fine mode particles ($r<1.0$ μm in the volume size distribution), hygroscopic aerosol particles (e.g., sulfates) have near neutral spectral dependence and high scattering efficiency [*Dubovik et al.*, 2002]. Black carbon (BC) particles have the strongest absorption in the near-

196 infrared (ω_o decreasing with λ when the sole absorber), while aerosols composed of brown
197 carbon (BrC) or organic carbon (OC) exhibit stronger absorption in ultraviolet and visible bands
198 (ω_o increasing with λ when the sole absorber) [*Eck et al.*, 2009]. Varying concentrations of BC
199 particles optically mixed with dust, BrC, and/or OC can produce ambiguous ω_o wavelength
200 dependence (i.e., increasing, decreasing, or constant with λ); however, the net effect is stronger
201 absorption across the retrieved spectrum (e.g., 440 to 1020 nm) [*Dubovik et al.*, 2002; *Giles et*
202 *al.*, 2011a].

203 The AERONET Version 2, Level 2.0 absorption properties at each site are presented in
204 Figure 2 and Table 2 to provide an update to *Dubovik et al.* [2002] and *Russell et al.* [2010]. The
205 spectral ω_o behavior is similar to *Dubovik et al.* [2002] for most regions. For Solar Village
206 (Dust), Capo Verde (Dust), GSFC (U/I), Mexico City (U/I), and Mongu (BB), the ω_o differences
207 between *Dubovik et al.* [2002] and Table 2 (i.e., $\omega_{o\ \text{Dubovik 2002}} - \omega_{o\ \text{Table 2}}$) showed an overall
208 average decrease of 0.01 for these sites with the largest decrease of 0.02 spectrally for GSFC and
209 Capo Verde and smallest decrease ranging from 0 to 0.01 for Mongu. Notably, the ω_o standard
210 deviations are significantly greater by 0.01 to 0.03 in the present study than *Dubovik et al.* [2002]
211 for all five sites. Table 2 differs from *Dubovik et al.* [2002] due to utilizing different analysis
212 criteria (e.g., $\tau_{440nm}>0.4$ in Table 2 vs. $\tau_{1020nm}\geq 0.3$ and $\alpha_{ext}\leq 0.6$ for desert dust in *Dubovik et al.*
213 [2002]), implementing improved surface characterization and inversion quality checks in
214 Version 2 (as discussed in Section 2), and utilizing a larger data set (e.g., the number of ω_o
215 retrievals at GSFC is four times larger than *Dubovik et al.* [2002]). For ω_{o440nm} as a function of
216 τ_{440nm}, the R^2 values—calculated based on a second order fit—ranged from 0.0 to 0.16 for each
217 site, indicating weak correlation and only up to 16% of ω_{o440nm} variation was explained by τ_{440nm}.
218 Table 2 shows that the Dust category has the least variability among sites likely due to the

similar mineral composition, while the BB category has the largest variability likely due to various fuel types and fuel combustion phases resulting from different relative BC emissions [*Eck et al*., 2003b]. The Mixed category ($0.33<\eta_{550nm}\leq 0.66$) ω_o average shows strong spectral absorption and dust-like ω_o spectra with stronger absorption at 440 nm due to significant dust contribution to the optical mixture. *Sokolik and Toon* [1998] showed that varying hematite amounts in dust can lead to increased absorption spectrally from the blue to near-infrared wavelength region. Using $\alpha_{ext}<0.2$ to designate "pure dust" as suggested by *Kim et al.* [2011], the overall "pure dust" average of ω_o for all Dust category sites is 0.91, 0.97, 0.97, 0.97 for the 440, 675, 870, and 1020 nm wavelengths, respectively. These "pure dust" ω_o values are lower by up to 0.02, spectrally, than those reported by *Dubovik et al.* [2002] for Dust sites and are lower by up to 0.01 for ω_o at 550 nm (logarithmically interpolated between 440 nm and 675 nm) compared to similar sites analyzed by *Kim et al.* [2011]. Table 2 shows the Dust site averages are lower than "pure dust," indicating possible incursions by other aerosols (e.g., biomass burning smoke). *Eck et al.* [2010] and *Giles et al.* [2011a] also showed increasing absorption with wavelength for decreasing α_{abs}, indicating an optical mixture and possibly aggregation of dust and carbonaceous particles at Kanpur, India. We interpolated η to 550 nm using the linear fit of the logarithms of τ_f, τ (i.e., $\tau_f + \tau_c$) and the 440, 675, and 870 nm wavelengths similar to *Lee et al.* [2010]. In Figure 3a, the Mixed category for the coarse mode particles (η_{550nm}: 0.0-0.33) resembles dust ω_o spectra as shown in Figure 2a. In Figure 3c, for fine mode particles (η_{550nm}: 0.66-1.0), the ω_o magnitudes and variability are similar to U/I or BB particle types categories but with less ω_o spectral dependence possibly due to varying amounts of BC, BrC, and OC [*Derimian et al.*, 2006; *Eck et al.*, 2009; 2010]. The average ω_o for α_{abs} binned between 1.5 and 2.0 shown by *Giles et al.* [2011a] at Kanpur closely resembles the absorption magnitude and

spectral shape of mixed aerosol types for the Mixed category ($0.33<\eta_{550nm}\leq 0.66$) in Table 2 as well as Figure 2b and Figure 3b suggesting various mixtures of aerosol particles contributing to the absorption.

The ω_o and τ_{ext} are used to derive the τ_{abs} from AERONET data. τ_{abs} and α_{abs} were averaged for each site based on dominant particle type category in Figure 4 and Table 2. For the five sites (Solar Village, Capo Verde, GSFC, Mexico City, and Mongu), a comparison of average α_{abs} values in Table 2 with *Russell et al.* [2010] for the 440-870 nm range shows the largest difference in α_{abs} (i.e., $\alpha_{abs\ Russell\ 2010} - \alpha_{abs\ Table\ 2}$) at GSFC (-0.25) and Capo Verde (+1.2). For the other three sites, the α_{abs} averages in Figure 4 are comparable to those reported by *Russell et al.* [2010] and *Giles et al.* [2011a]. In Figure 5, the Mixed category was further stratified by the η_{550nm} as in Figure 3. The coarse particle range (η_{550nm}: 0.0-0.33) shows similar α_{abs} (1.7-2.3) as the Dust category (which is expected for dust dominated cases) and the fine particle range (η_{550nm}: 0.66-1.0) shows an α_{abs} (0.8-1.5) similar to BB and U/I categories. The mixed size particle range (η_{550nm}: 0.33-0.66) is nearly identical to the Mixed category α_{abs} (1.2-1.7) in Figure 4b and similar to values reported by *Eck et al.* [2010]. As shown by *Bergstrom et al.* [2007] and *Russell et al.* [2010], the α_{abs} may vary significantly when considering the aerosol particle size between fine and coarse modes; however, when considering U/I and BB aerosols within the fine particle range, significant overlap results in α_{abs}. The sensitivity of α_{abs} with respect to input parameters will be investigated in the next section.

3.2 Absorption Ångström Exponent Sensitivity Study

The retrieved values of α_{abs} have a normal distribution (Figure 6) when calculating α_{abs} using three wavelengths (440-675-870 nm) for each dominant aerosol type. *Russell et al.* [2010] showed that the average α_{abs} values generally decreased with increasing spectral range possibly

265 due in part to the crude surface reflectance assumption made in early AERONET analysis (as
266 discussed in Section 3.1), while *Gyawali et al.* [2012] showed an increasing α_{abs} values with
267 increasing spectral range for clean and polluted days during winter in Reno, Nevada. However,
268 increasing or decreasing trends of α_{abs} depend on the wavelength interval [*Lack and Cappa*
269 2010]. These α_{abs} values computed from 440-675-870 nm wavelength range have large
270 variability with standard deviations ranging from ±0.3 to ±0.6 (1.76±0.58 for Dust; 1.53±0.44 for
271 Mixed; 1.21±0.37 for U/I; 1.35±0.35 for BB). Individual α_{abs} retrieval calculations [α_{abs} (Dust):
272 ~0-4; α_{abs} (Mixed): ~0-3.5; α_{abs} (U/I): ~0-2; α_{abs} (BB): ~0-2.5] are within the range of all
273 dominant particle types; therefore, α_{abs} should not be used alone to determine aerosol types
274 without the use of other information (e.g., aerosol size). Further, Figure 6 shows a significant
275 percentage of α_{abs} below 1.0, which is the black carbon limit for very small particles [*Bergstrom*
276 *et al*., 2002]. However, *Lack and Cappa* [2010] suggested α_{abs} (from 380-750 nm) values for
277 larger optically effective BC particles may exist between ~-0.2 and 1.6 depending on the BC
278 coating material. Nonetheless, the U/I category has over 22% of the α_{abs} retrievals below 1.0,
279 while the other categories have ~10% of the data below α_{abs} of 1.0 also possibly due to the
280 uncertainty of the retrieved ω_o.

281 A sensitivity study of α_{abs} was performed to test the response of α_{abs} by varying ω_o for
282 each wavelength (i.e., 440, 675, and 870 nm) and holding τ_{ext} constant (i.e., AOD cannot be
283 perturbed since it is used in the calculation of ω_o retrieval). First, ω_o was varied by ±0.03, the
284 current AERONET ω_o uncertainty estimate [*Dubovik et al*., 2002]. Additional tests included
285 varying ω_o by ±0.01, ±0.02, and ±0.04 to show the variability of α_{abs} with various degrees of ω_o
286 uncertainty. Different spectral ω_o inputs schemes were implemented to determine the α_{abs}
287 response by varying ω_o equally across all wavelengths, by perturbing ω_o at only one end point in

288 the 440-675-870 nm wavelength set (i.e., 440 nm or 870 nm), and by perturbing ω_o at 440 nm or
289 870 nm in the 440-870 nm wavelength pair (i.e., excluding 675 nm). Positive ω_o perturbation
290 may approach values of 1.0 (i.e., absolute scattering) and can produce large positive or negative
291 α_{abs} due to very low τ_{abs}. To prevent such cases, the ω_o magnitude was limited to less than 0.995
292 for positive ω_o perturbations for all wavelengths resulting in a reduced data subset.

293 Table 3 shows the sensitivity of α_{abs} to perturbations in ω_o. The perturbation of ± 0.03 ω_o
294 (the current estimated uncertainty) changed α_{abs} by at least ~$\pm$0.6 for Dust, ~$\pm$0.2 for Mixed, and
295 ~$\pm$0.1 for U/I and BB. The perturbations of ω_o by ± 0.02 showed ~0.1 smaller corresponding
296 change in α_{abs} with respect to ± 0.03 ω_o perturbations for Dust and less than 0.05-0.10 for the
297 other categories. Perturbations of ω_o by ± 0.04 showed large deviations from the unperturbed
298 data set, indicating much greater uncertainty for α_{abs} with increasing ω_o uncertainty. The
299 simulated overestimation of spectral ω_o for U/I and BB (i.e., $\delta\omega_o$=-0.03) showed a higher $\delta\alpha_{abs}$
300 suggesting a possibility that the unperturbed α_{abs} is underestimated and may possibly, at least
301 partly, explain α_{abs} below 1.0 in these categories. However, *Lack and Cappa* [2010] determined
302 that the large α_{abs} variation (-0.2 and 1.3 for the 380-750 nm wavelength range) for BC particles
303 with coatings are possible and α_{abs} values less than 1.0 may occur with larger BC particles (e.g.,
304 r_{core}>0.1 μm and r_{shell}>0.25 μm). *Gyawali et al.* [2012] showed laboratory measurements of
305 kerosene soot particles have α_{abs} values of ~0.8 for the 355-1020 nm range and in situ
306 measurement values of α_{abs} measured during the Reno, Nevada, winter period varied for clean
307 days ($PM_{2.5}$<40 μg/m^3) between ~1.0 and 1.4 and for polluted days ($PM_{2.5}\geq$40 μg/m^3) between
308 0.9 and 1.2 for the 405-870 nm wavelength range. Although these model simulations and
309 laboratory and in situ measurements suggest α_{abs} values may occur below 1.0, AERONET
310 remotely sensed values of α_{abs} have not yet been compared to coincident column-effective in situ

311 measurements (e.g., measured by aircraft) but this analysis will be addressed in future work. In
312 the present analysis, the simulated underestimation of spectral ω_o (i.e., $\delta\omega_o$=+0.03) for Dust and
313 Mixed indicates possible underestimation of the unperturbed α_{abs}, which could also result in α_{abs}
314 below 1.0. Table 3 also shows the Dust and Mixed categories change in the same direction as
315 the ω_o perturbation possibly due to weak spectral dependence of τ_{ext}, while U/I and BB
316 categories have the opposite response. Two additional tests were conducted by perturbing ω_o
317 using the wavelength pair (440-870 nm) and only varying the end points of the 440-675-870 nm
318 set and the differences between unperturbed α_{abs} averages were minimal (not shown). However,
319 perturbing one ω_o end point for either the 440-870 nm wavelength pair (not shown) or the 440-
320 675-870 nm set (Table 3) produced very large deviations in α_{abs} by up to ~1.2 for Dust, ~0.7 for
321 Mixed, ~1.0 for U/I, and ~0.6 for BB. The perturbation of end points simulates atypical behavior
322 of the instrument while deployed in the field (e.g., anomalous filter degradation) showing
323 potential issues in using real-time data products unless further screening is implemented, such as
324 the instrument collimator consistency checks (stated in Section 2.0), which may be utilized to
325 help remove ω_o artifacts (i.e., collimator or sensor head window obstructions) and improve the
326 reliability of α_{abs} retrievals. These sensitivity tests quantified the effect of the reduction of ω_o
327 uncertainty on improving estimates of α_{abs}.

328 **3.3 Cluster Analysis by Dominant Aerosol Type**

329 Knowledge of aerosol particle spectral absorption provides insight to determine aerosol
330 particle dominance of dust, carbonaceous matter, or hygroscopic aerosols (e.g., sulfates, nitrates,
331 or sea salt). While the co-albedo (or 1-ω_o) indicates the magnitude of absorption and α_{abs}
332 provides some indication of the dominance of carbonaceous particles (e.g., BC, BrC, and OC) or
333 iron oxides in dust, these parameters alone cannot fully describe the aerosol particle type.

Recent studies have suggested applying an aerosol particle size parameter (e.g., α_{ext} or η) to separate larger dust particles from other aerosol types and mixtures [*Lee et al*., 2010; *Russell et al*., 2010; *Giles et al.*, 2010; 2011a; 2011b]. In this section, several years of AERONET retrievals of ω_{o440nm}, $\alpha_{abs440\text{-}870nm}$, $\alpha_{ext440\text{-}870nm}$, and η_{550nm} (with wavelength subscripts removed hereafter) were analyzed for each dominant aerosol type category using a density based clustering utilizing the Voronoi tessellation [*Voronoi* 1908; *Ishimoto et al*., 2010] to determine the relative concentration of points (density = 1/polygon area) for each absorption and size relationship. In these density plots (e.g., Figures 7-10), the high density represents the primary mode for the dominant aerosol particle type category. Various clustering techniques were attempted previously to categorize dominant aerosol particle type at AERONET sites [*Cattrall et al*., 2005; *Omar et al*., 2005; *Levy et al*., 2007; *Qin and Mitchell* 2009; *Russell et al*., 2010, *Boselli et al*., 2012]. For each absorption and size relationship and aerosol type category in this study (Figure 11), dominant aerosol particle clusters were computed using averages weighted by density magnitudes normalized to a 64-level scale (corresponding to a 64-bit color scale). Although weighting reduces the bias introduced by outliers affecting the normal average, additional thresholds were applied to the aerosol size parameters. To further define weighted cluster averages, the α_{ext} cluster averages utilized a 0.8 threshold, where >0.8 indicates mainly small sub-micron radius particles and ≤0.8 is mainly large super-micron radius particles (where $\alpha_{ext440\text{-}870nm}$=0.8 is approximately equivalent to η_{500nm}=0.5 as shown for example by *Eck et al.* [2005; 2010]). In addition, the η cluster averages were defined using thresholds of 0.0 to ≤0.33 (for coarse mode dominated particles), 0.33 to ≤0.66 (for mixed size), and >0.66 (for fine mode dominated particles). For the BB category (Figure 11c and Figure 11d), cluster separation was

imposed to calculate two additional clusters using a ω_{o440nm} threshold of 0.90 based on the density cluster analyses shown in Figure 9 and Figure 10.

The relationships of aerosol absorption and size are analyzed with respect to the dominant aerosol type category. For Figures 7-10, the primary density clusters are clear (denoted by orange and red regions representing relative value levels of ~45 to 64). For example, the Dust category shows a cluster in the region with α_{ext} of ~0.2-0.3 and η of ~0.2-0.3, indicative of domination by coarse mode particles. To provide a better assessment of the clusters, the weighted cluster average and one standard deviation was calculated for each parameter shown in Figure 11. In Figure 11a and Figure 11b, the primary Dust clusters show variation of the α_{abs} mainly between 1.5 and 2.3, which are slightly lower values than reported by *Russell et al.* [2010]. In Figure 11c and Figure 11d, ω_o also varies significantly in the primary Dust cluster from 0.89-0.93, possibly due to variation in mineral composition of dust [*Sokolik and Toon* 1999]. For α_{ext} (Figure 11a and Figure 11c), the Mixed aerosol type category has two primary density clusters (1) "Mixed-Large Particle" cluster for mainly super-micron particles (centered at α_{ext}~0.4) and (2) "Mixed-Small Particle" for mainly submicron particles (centered at α_{ext}~1.25). In comparison to the Dust cluster, the Mixed-Large Particle cluster tends to have a slightly smaller contribution to larger particles in the 0.3-0.6 α_{ext} range, while η relationships (Figure 11b and Figure 11d) show the Mixed-Large Particle cluster for coarse particles is nearly identical to the Dust cluster. The Mixed category for mixed sizes ($0.33<\eta_{550nm}\leq0.66$) does not show high cluster density due to varying sizes and contributions of the aerosol particles containing dust with pollution or biomass burning smoke with strongly varying absorption [*Eck et al.*, 2010]. In Figure 11, the Mixed-Small Particle clusters (α_{ext}~1.0 to 1.5; also η~0.8-0.95) show significant variability likely due to variation in carbonaceous particle contribution

(primarily BC but also OC) with α_{abs} between ~1.3 and 1.7 similar to those observed in Kanpur for fine mode dominated cases by *Giles et al.* [2011a]. As indicated by *Russell et al.* [2010] and shown in Figure 6, the U/I and BB category types for the α_{abs} and α_{ext} relationship tend to overlap each other. For primary density clusters in these two categories, the α_{abs} vary from ~1.1 to 1.8. Until the ω_o uncertainty is known and constrained further (given the sensitivity results of Section 3.2), the usefulness of α_{abs} to determine various carbonaceous aerosol particles is doubtful except in separating cases dominated by BC from cases dominated by BrC or OC. A "region" of higher α_{abs} values from the density cluster analysis for BB (Figure 7d and Figure 8d) likely indicates aged smoke from primarily smoldering combustion containing higher concentrations of BrC or OC and relatively low BC [*Eck et al.*, 2009; *Moosmüller et al*., 2009; 2011], especially above an α_{abs} of 1.6 for fine mode particles [*Lack and Cappa* 2010] and also supported by Figure 9d and Figure 10d with ω_o above 0.90. For example, according to *Eck et al.* [2009] and *Arola et al.* [2011], significant absorbing OC concentrations and high OC/BC ratios likely occurred at the Bonanza Creek site where Table 2 shows the spectral ω_o average is ~0.95 and averages of α_{abs}, α_{ext}, and η_{550nm} are 1.8, 1.5, and 0.96, respectively. However, the ω_o relationships (Figure 11c and Figure 11d) show more cluster separation than α_{abs} relationships (Figure 11a and Figure 11b). In Figure 11d, the primary U/I cluster is centered above 0.95, while the main BB cluster is centered on ~0.89 with two BB sub-clusters centered on ~0.93 and ~0.87 ω_o (calculated by using ω_o threshold of 0.90); however, the BB clusters overlap with the Mixed-Small Particle cluster. The ω_{o440nm} and $\alpha_{ext440\text{-}870\ nm}$ relationship (Figure 11c) shows distinct high density clusters in all categories (i.e., between Dust and Mixed-Large Particle, and among Mixed-Small Particle-U/I-BB, and between U/I-BB clusters), while minimal overlap occurs with the U/I and the less absorbing (ω_o>0.90) BB sub-cluster. Nonetheless, the analysis has shown that the ω_{o440nm} and

$\alpha_{ext440\text{-}870\ nm}$ relationship demonstrates that the dominant particle type may be ascertained simply from commonly measured or retrieved absorption and size parameters.

4.0 Conclusions

In this paper, absorption properties (i.e., single scattering albedo and absorption Ångström exponent) were averaged for 19 AERONET sites to show correspondence to representative aerosol source regions. Sensitivity tests on absorption Ångström exponent were performed by varying the single scattering albedo within plausible constraints based on uncertainty estimates. Lastly, the absorption and size relationships were evaluated and compared to each other based on the dominant aerosol type categorizations.

(1) A summary of aerosol absorption parameters from the AERONET Version 2, Level 2.0 almucantar retrievals was presented to expand upon previous work using pre-Version 1 retrievals. A comparison of five sites common to *Dubovik et al.* [2002] showed a 0.01 average spectral (from 440 to 1020 nm) decrease in single scattering albedo (ω_o) with the largest decreases spectrally of 0.02 at Capo Verde and GSFC AERONET sites. The average absorption Ångström exponent ($\alpha_{abs440\text{-}870\ nm}$) computed from Version 2 retrievals was 1.2 lower for Capo Verde and 0.25 higher for GSFC than reported by *Russell et al.* [2010] computed from pre-Version 1 retrievals. Aerosol mixtures exhibited stronger spectral absorption (i.e., lower ω_o) and increased dominance of absorbing carbonaceous particles (i.e., lower $\alpha_{abs440\text{-}870\ nm}$) than for dust alone, possibly due to an optical mixture state (e.g., dust and smoke or dust and pollution) or the aggregation of dust and carbonaceous particles.

(2) The $\alpha_{abs440\text{-}870\ nm}$ calculated from AERONET data ranged from ~0 to 3.5 among dominant aerosol type categories. Frequency distributions of $\alpha_{abs440\text{-}870\ nm}$ exhibited significant

overlap among aerosol types, while the Urban/Industrial and Biomass Burning distributions were nearly identical for $\alpha_{abs440\text{-}870\ nm}$ values above 1.0. Further, frequency distributions showed approximately 10% of the α_{abs} retrievals had values below 1.0 for most aerosol categories but as high as 22% for the Urban/Industrial category.

(3) A sensitivity study perturbing the ω_o by the current AERONET uncertainty (±0.03) showed α_{abs} changes by at least ~±0.6 for Dust, ~±0.2 for Mixed, and ~±0.1 for Urban/Industrial and Biomass Burning. The sensitivity study quantified the improvement in estimates of α_{abs} resulting from reducing the ω_o uncertainty. Variations within the uncertainty of ω_o retrievals may explain some of the observed α_{abs} values below 1.0 in AERONET data although in situ measurements suggest that some of these α_{abs} values may be real depending on the aerosol particle composition and size.

(4) Absorption and size relationships were examined using density cluster analysis for each dominant aerosol particle type. The ω_{o440nm} vs. $\alpha_{ext440\text{-}870\ nm}$ relationship showed at least five distinct aerosol type clusters [Dust, Mixed-Large Particle, Mixed-Small Particle, Urban/Industrial, and Biomass Burning (with two sub-clusters)], while the $\alpha_{abs440\text{-}870\ nm}$ vs. $\alpha_{ext440\text{-}870\ nm}$ relationship had fewer distinct clusters due to less definition for mainly small aerosol particles ($\alpha_{ext440\text{-}870\ nm}$>1.5).

We showed the ω_{o440nm} and $\alpha_{ext440\text{-}870nm}$ relationship provided a better clustering relationship and it may be applied to measurements of aerosol absorption and size properties derived from surface- and potentially future space-based platforms. From ω_{o440nm} and $\alpha_{ext440\text{-}870\ nm}$ clusters, at least, major dominant aerosols types and some mixtures can be identified using common aerosol absorption and size parameters without prior knowledge of aerosol transport or

source regions. Alternatively, when ω_o is not available but $\alpha_{abs440\text{-}870nm}$ is (e.g., using spectral absorption coefficients measured in situ to calculate α_{abs}), $\alpha_{abs440\text{-}870nm}$ vs. $\alpha_{ext440\text{-}870nm}$ may also provide a reasonable aerosol type classification. A combination of ω_{o440nm} vs. $\alpha_{ext440\text{-}870nm}$ and $\alpha_{abs440\text{-}870nm}$ vs. $\alpha_{ext440\text{-}870nm}$ relationships could provide a more detailed classification of aerosol composition which will require further investigation.

5.0 Acknowledgements

The NASA AERONET project is supported by the NASA EOS project office, and the Radiation Sciences Program, NASA Headquarters. We would like to thank the following principal investigators and their staff for maintaining the following sites: Didier Tanre (Banizoumbou, Capo Verde, Dakar, and Ouagadougou), Naif Al-Abbadi (Solar Village), Rachel Pinker (Ilorin), Sachi Tripathi and Ramesh Singh (Kanpur), Arnon Karnieli (SEDE BOKER), Pucai Wang (XiangHe), Giuseppe Zibordi (Ispra), Amando L. Contreras (Mexico City), Alexander Aculinin (Moldova), Itaru Sano (Shirahama), Paulo Artaxo (Abracos Hill, Alta Floresta), John Vande Castle (Bonanza Creek), and Ross Mitchell (Lake Argyle). Finally, the authors thank the AERONET team for calibrating and maintaining instrumentation and processing these data.

References

Ångström, A. (1964), The parameters of atmospheric turbidity, *Tellus*, *16*(1), 64–75.

Arola, A., Schuster, G., Myhre, G., Kazadzis, S., Dey, S., and Tripathi, S. N. (2011), Inferring absorbing organic carbon content from AERONET data, Atmos. Chem. Phys., 11, 215-225, doi:10.5194/acp-11-215-2011.

Basart, S., Pérez, C., Cuevas, E., Baldasano, J. M., and Gobbi, G. P. (2009), Aerosol characterization in Northern Africa, Northeastern Atlantic, Mediterranean Basin and Middle East from direct-sun AERONET observations, *Atmos. Chem. Phys.*, *9*, 8265-8282, doi:10.5194/acp-9-8265-2009.

Bergstrom, R. W., P. B. Russell, and P. Hignett (2002), Wavelength dependence of the absorption of black carbon particles: Predictions and results from the TARFOX experiment and implications for the aerosol single scattering albedo, *J. Atmos. Sci.*, *59*, 567–577, doi:10.1175/1520-0469(2002) 059<0567:WDOTAO>2.0.CO;2.

Bergstrom, R. W., P. Pilewskie, P. B. Russell, J. Redemann, T. C. Bond, P. K. Quinn, and B. Sierau (2007), Spectral absorption properties of atmospheric aerosols, *Atmos. Chem. Phys.*, *7*, 5937–5943, doi:10.5194/acp-7-5937-2007.

Boselli A., R. Caggiano, C. Cornacchia, F. Madonna, L. Mona, M. Macchiato, G. Pappalardo, and S. Trippetta (2012), Multi year sun-photometer measurements for aerosol characterization in a Central Mediterranean site, *J. Atmos. Res.*, *104-105*, 98-110, doi: 10.1016/j.atmosres.2011.08.002.

Burton, S. P., Ferrare, R. A., Hostetler, C. A., Hair, J. W., Rogers, R. R., Obland, M. D., Butler, C. F., Cook, A. L., Harper, D. B., and Froyd, K. D. (2012), Aerosol classification using airborne High Spectral Resolution Lidar measurements – methodology and examples, Atmos. Meas. Tech., 5, 73-98, doi:10.5194/amt-5-73-2012.

Cattrall, C., J. Reagan, K. Thome, and O. Dubovik (2005), Variability of aerosol and spectral lidar and backscatter and extinction ratios of key aerosol types derived from selected Aerosol Robotic Network locations, *J. Geophys. Res.*, *110*, D10S11, doi:10.1029/2004JD005124.

Derimian, Y., A. Karnieli, Y. J. Kaufman, M. O. Andreae, T. W. Andreae, O. Dubovik, W. Maenhaut, I. Koren, and B. N. Holben (2006), Dust and pollution aerosols over the Negev desert, Israel: Properties, transport, and radiative effect, *J. Geophys. Res.*, *111*, D05205, doi:10.1029/2005JD006549.

Derimian, Y., A. Karnieli, Y. J. Kaufman, M. O. Andreae, T. W. Andreae, O. Dubovik, W. Maenhaut, and I. Koren (2008), The role of iron and black carbon in aerosol light absorption, *Atmos. Chem. Phys.*, *8*, 3623–3637, doi:10.5194/acp-8-3623-2008.

Dey, S., S. N. Tripathi, R. P. Singh, and B. N. Holben (2004), Influence of dust storms on the aerosol optical properties over the Indo-Gangetic basin, *J. Geophys. Res.*, *109*, D20211, doi:10.1029/2004JD004924.

Diner, D. J., G. P. Asner, R. Davies, Y. Knyazikhin, J.-P. Muller, A. W. Nolin, B. Pinty, C. B. Schaaf, and J. Stroeve (1999), New Directions in Earth Observing: Scientific Applications of Multiangle Remote Sensing, *Bull. Amer. Meteor. Soc.*, *80*, 2209–2228, doi: http://dx.doi.org/10.1175/1520-0477(1999)080<2209:NDIEOS>2.0.CO;2.

Dubovik, O., and M. D. King (2000), A flexible inversion algorithm for retrieval of aerosol optical properties from Sun and sky radiance measurements, *J. Geophys. Res.*, *105*, 20,673–20,696, doi:10.1029/2000JD900282.

Dubovik, O., A. Smirnov, B. N. Holben, M. D. King, Y. J. Kaufman, T. F. Eck, and I. Slutsker (2000), Accuracy assessments of aerosol optical properties retrieved from AERONET Sun and sky-radiance measurements, *J. Geophys. Res.*, *105*, 9791–9806, doi:10.1029/2000JD900040.

Dubovik, O., B. N. Holben, T. F. Eck, A. Smirnov, Y. J. Kaufman, M. D. King, D. Tanre, and I. Slutsker (2002), Variability of absorption and optical properties of key aerosol types observed in worldwide locations, *J. Atmos. Sci.*, *59*, 590–608, doi:10.1175/1520-0469(2002)059<0590:VOAAOP>2.0.CO;2.

Dubovik, O., et al. (2006), Application of spheroid models to account for aerosol particle nonsphericity in remote sensing of desert dust, *J. Geophys. Res.*, *111*, D11208, doi:10.1029/2005JD006619.

Eck, T. F., B. N. Holben, J. S. Reid, O. Dubovik, A. Smirnov, N. T. O'Neill, I. Slutsker, and S. Kinne (1999), Wavelength dependence of the optical depth of biomass burning, urban, and desert dust aerosols, *J. Geophys. Res.*, *104*(D24), 31,333–31,349, doi:10.1029/1999JD900923.

Eck, T. F., et al. (2003a), Variability of biomass burning aerosol optical characteristics in southern Africa during the SAFARI 2000 dry season campaign and a comparison of single scattering albedo estimates from radiometric measurements, *J. Geophys. Res.*,*108*(D13), 8477, doi:10.1029/2002JD002321.

Eck, T. F., B. N. Holben, J. S. Reid, N. T. O'Neill, J. S. Schafer, O. Dubovik, A. Smirnov, M. A. Yamasoe, and P. Artaxo (2003b), High aerosol optical depth biomass burning events: A comparison of optical properties for different source regions, *Geophys. Res. Lett.*, *30*(20), 2035, doi:10.1029/2003GL017861.

Eck, T. F., et al. (2005), Columnar aerosol optical properties at AERONET sites in central eastern Asia and aerosol transport to the tropical mid-Pacific, *J. Geophys. Res.*, *110*, D06202, doi:10.1029/2004JD005274.

Eck, T. F., et al. (2008), Spatial and temporal variability of column-integrated aerosol optical properties in the southern Arabian Gulf and United Arab Emirates in summer, *J. Geophys. Res.*, *113*, D01204, doi:10.1029/2007JD008944.

536 Eck, T. F., et al. (2009), Optical properties of boreal region biomass burning aerosols in central
537 Alaska and seasonal variation of aerosol optical depth at an Arctic coastal site, *J.*
538 *Geophys. Res.*, *114*, D11201, doi:10.1029/2008JD010870.

539 Eck, T. F., et al. (2010), Climatological aspects of the optical properties of fine/coarse mode
540 aerosol mixtures, *J. Geophys. Res.*, *115*, D19205, doi:10.1029/2010JD014002.

541 Giles, D. M., B. Hoblen, T. F. Eck, A. Sinyuk, R.R. Dickerson, A. M. Thompson, I. Slutsker, Z.
542 Li, S. N. Tripathi, R. Singh, and G. Zibordi (2010), Identifying Aerosol Type/Mixture
543 from Aerosol Absorption Properties Using AERONET, *Eos Trans. AGU*, *91*(26), West.
544 Pac. Geophys. Meet. Suppl., Abstract A33D-05.

545 Giles, D. M., et al. (2011a), Aerosol properties over the Indo-Gangetic Plain: A mesoscale
546 perspective from the TIGERZ experiment, *J. Geophys. Res.*, *116*, D18203,
547 doi:10.1029/2011JD015809.

548 Giles, D. M., B. N. Holben, T. F. Eck, A. Sinyuk, A. Smirnov, I. Slutsker, R. R. Dickerson, A.
549 M. Thompson, and J. S. Schafer (2011b), Dominant Aerosol Particle Type/Mixture
550 Identification at Worldwide Locations Using the Aerosol Robotic Network (AERONET),
551 Abstract A14E-07 presented at 2011 Fall Meeting, AGU, San Francisco, Calif., 5-9 Dec.

552 Gobbi, G. P., Kaufman, Y. J., Koren, I., and Eck, T. F. (2007), Classification of aerosol
553 properties derived from AERONET direct sun data, *Atmos. Chem. Phys.*, *7*, 453-458,
554 doi:10.5194/acp-7-453-2007.

555 Gyawali, M., et al. (2012), Photoacoustic optical properties at UV, VIS, and near IR wavelengths
556 for laboratory generated and winter time ambient urban aerosols, *Atmos. Chem. Phys.*, *12*,
557 2587-2601, doi:10.5194/acp-12-2587-2012.

558 Holben, B. N., T. F. Eck, and R. S. Fraser (1991), Temporal and spatial variability of aerosol
559 optical depth in the Sahel region in relation to vegetation remote sensing, *Int. J. Remote*
560 *Sens.*, *12*(6), 1147–1163, doi:10.1080/01431169108929719.

561 Holben, B. N., et al. (1998), AERONET–A federated instrument network and data archive for
562 aerosol characterization, *Remote Sens. Environ.*, *66*, 1–16, doi:10.1016/S0034-
563 4257(98)00031-5.

564 Holben, B. N., et al. (2001), An emerging ground-based aerosol climatology: Aerosol optical
565 depth from AERONET, *J. Geophys. Res.*, *106*(D11), 12,067–12,097,
566 doi:10.1029/2001JD900014.

567 Holben, B. N., T. F. Eck, I. Slutsker, A. Smirnov, A. Sinyuk, J. Schafer, D. Giles, and O.
568 Dubovik (2006), AERONET's Version 2.0 quality assurance criteria, in Remote Sensing
569 of the Atmosphere and Clouds, edited by S.-C. Tsay et al., *Proc. SPIE*, *6408*, 64080Q,
570 doi:10.1117/12.706524.

571 Ishimoto, H., Y. Zaizen, A. Uchiyama, K. Masuda, Y. Mano (2010), Shape modeling of mineral
572 dust particles for light-scattering calculations using the spatial Poisson–Voronoi
573 tessellation, *J. of Quant. Spect. and Rad. Trans.*, *111*, 16, doi:10.1016/j.jqsrt.2010.06.018.

574 Jeong, M.-J., and Z. Li (2005), Quality, compatibility, and synergy analyses of global aerosol
575 products derived from the advanced very high resolution radiometer and Total Ozone
576 Mapping Spectrometer, *J. Geophys. Res.*, *110*, D10S08, doi:10.1029/2004JD004647.

577 Johnson, B. T., S. Christopher, J. M. Haywood, S. R. Osborne, S. McFarlane, C. Hsu, C.
578 Salustro, and R. Kahn (2009), Measurements of aerosol properties from aircraft and
579 ground-based remote sensing: A case-study from the Dust and Biomass-burning
580 Experiment (DABEX), *Q. J. R. Met. Soc.*, *135*, doi:10.1002/qj.420.

581 Kahn, R. A., B. J. Gaitley, M. J. Garay, D. J. Diner, T. F. Eck, A. Smirnov, and B. N. Holben
582 (2010), Multiangle Imaging SpectroRadiometer global aerosol product assessment by
583 comparison with the Aerosol Robotic Network, *J. Geophys. Res.*, *115*, D23209,
584 doi:10.1029/2010JD014601.

585 Kalapureddy, M. C. R., D. G. Kaskaoutis, P. Ernest Raj, P. C. S. Devara, H. D. Kambezidis, P.
586 G. Kosmopoulos, and P. T. Nastos (2009), Identification of aerosol type over the Arabian
587 Sea in the premonsoon season during the Integrated Campaign for Aerosols, Gases and
588 Radiation Budget (ICARB), *J. Geophys. Res.*, *114*, D17203, doi:10.1029/2009JD011826.

589 Kaufman, Y. J., A. Setzer, D. Ward, D. Tanre, B. N. Holben, P. Menzel, M. C. Pereira, and R.
590 Rasmussen (1992), Biomass Burning Airborne and Spaceborne Experiment in the
591 Amazonas (BASE-A), *J. Geophys. Res.*, *97*(D13), 14,581–14,599,
592 doi:10.1029/92JD00275.

593 Kim, D., Chin, M., Yu, H., Eck, T. F., Sinyuk, A., Smirnov, A., and Holben, B. N. (2011), Dust
594 optical properties over North Africa and Arabian Peninsula derived from the AERONET
595 dataset, *Atmos. Chem. Phys.*, *11*, 10733-10741, doi:10.5194/acp-11-10733-2011.

596 Lack, D. A. and Cappa, C. D. (2010), Impact of brown and clear carbon on light absorption
597 enhancement, single scatter albedo and absorption wavelength dependence of black
598 carbon, *Atmos. Chem. Phys.*, *10*, 4207-4220, doi:10.5194/acp-10-4207-2010.

599 Leahy, L. V., T. L. Anderson, T. F. Eck, and R. W. Bergstrom (2007), A synthesis of single
600 scattering albedo of biomass burning aerosol over southern Africa during SAFARI 2000,
601 *Geophys. Res. Lett.*, *34*, L12814, doi:10.1029/2007GL029697.

602 Lee J., J. Kim, C.H. Song, S.B. Kim, Y. Chun, B.J. Sohn, and B.N. Holben (2010),
603 Characteristics of aerosol types from AERONET sunphotometer measurements, *Atmos.*
604 *Environ.*, *44*, 26, doi: 10.1016/j.atmosenv.2010.05.035.

605 Levy, R. C., L. A. Remer, and O. Dubovik (2007), Global aerosol optical properties and
606 application to Moderate Resolution Imaging Spectroradiometer aerosol retrieval over
607 land, *J. Geophys. Res.*, *112*, D13210, doi:10.1029/2006JD007815.

608 Mélin, F., and G. Zibordi (2005), Aerosol variability in the Po Valley analyzed from automated
609 optical measurements, *Geophys. Res. Lett.*, *32*, L03810, doi:10.1029/2004GL021787.

610 Mielonen, T., A. Arola, M. Komppula, J. Kukkonen, J. Koskinen, G. de Leeuw, and K. E. J.
611 Lehtinen (2009), Comparison of CALIOP level 2 aerosol subtypes to aerosol types

612 derived from AERONET inversion data, *Geophys. Res. Lett.*, *36*, L18804,
613 doi:10.1029/2009GL039609.

614 Mitchell, R. M., D. M. O'Brien, and S. K. Campbell (2006), Characteristics and radiative impact
615 of the aerosol generated by the Canberra firestorm of January 2003, *J. Geophys. Res.*,
616 *111*, D02204, doi:10.1029/2005JD006304.

617 Moosmüller H., R. K. Chakrabarty, W. P. Arnott (2009), Aerosol light absorption and its
618 measurement: A review, *J. of Quant. Spect. and Rad. Trans.*, *110*, 11,
619 doi:10.1016/j.jqsrt.2009.02.035.

620 Moosmüller, H., Chakrabarty, R. K., Ehlers, K. M., and Arnott, W. P. (2011), Absorption
621 Ångström coefficient, brown carbon, and aerosols: basic concepts, bulk matter, and
622 spherical particles, *Atmos. Chem. Phys.*, *11*, 1217-1225, doi:10.5194/acp-11-1217-2011.

623 Müller, D., et al. (2010), Mineral dust observed with AERONET Sun photometer, Raman lidar,
624 and in situ instruments during SAMUM 2006: Shape-independent particle properties, *J.*
625 *Geophys. Res.*, *115*, D07202, doi:10.1029/2009JD012520.

626 Omar, A. H., J.-G. Won, D. M. Winker, S.-C. Yoon, O. Dubovik, and M. P. McCormick (2005),
627 Development of global aerosol models using cluster analysis of Aerosol Robotic Network
628 (AERONET) measurements, *J. Geophys. Res.*, *110*, D10S14,
629 doi:10.1029/2004JD004874.

630 O'Neill, N. T., S. Thulasiraman, T. F. Eck, and J. S. Reid (2005), Robust optical features of fine
631 mode size distributions: Application to the Québec smoke event of 2002, *J. Geophys.*
632 *Res.*, *110*, D11207, doi:10.1029/2004JD005157.

633 Prasad, A. K., and R. P. Singh (2007), Changes in aerosol parameters during major dust storm
634 events (2001–2005) over the Indo-Gangetic Plains using AERONET and MODIS data, *J.*
635 *Geophys. Res.*, *112*, D09208, doi:10.1029/2006JD007778.

636 Qin, Y. and Mitchell, R. M. (2009), Characterisation of episodic aerosol types over the
637 Australian continent, *Atmos. Chem. Phys.*, *9*, 1943-1956, doi:10.5194/acp-9-1943-2009.

638 Reid, J. S., T. F. Eck, S. A. Christopher, P. V. Hobbs, and B. Holben (1999), Use of the
639 Ångstrom exponent to estimate the variability of optical and physical properties of aging
640 smoke particles in Brazil, *J. Geophys. Res.*, *104*(D22), 27,473–27,489,
641 doi:10.1029/1999JD900833.

642 Reid, J. S., et al (2003)., Analysis of measurements of Saharan dust by airborne and ground-
643 based remote sensing methods during the Puerto Rico Dust Experiment (PRIDE), *J.*
644 *Geophys. Res.*, *108*(D19), 8586, doi:10.1029/2002JD002493.

645 Russell, P. B., R. W. Bergstrom, Y. Shinozuka, A. D. Clarke, P. F. DeCarlo, J. L. Jimenez, J. M.
646 Livingston, J. Redemann, O. Dubovik, and A. Strawa (2010), Absorption Ångstrom
647 Exponent in AERONET and related data as an indicator of aerosol composition, *Atmos.*
648 *Chem. Phys.*, *10*, 1155–1169, doi:10.5194/acp-10-1155-2010.

Sano, I., S. Mukai, Y. Okada, B. N. Holben, S. Ohta, and T. Takamura (2003), Optical properties of aerosols during APEX and ACE-Asia experiments, *J. Geophys. Res.*, *108*(D23), 8649, doi:10.1029/2002JD003263.

Satheesh, S. K., K. K. Moorthy (2005), Radiative effects of natural aerosols: A review, *Atmos. Environ.*, *39*, 11, 2089-2110, doi:10.1016/j.atmosenv.2004.12.029.

Schafer, J. S., T. F. Eck, B. N. Holben, P. Artaxo, and A. F. Duarte (2008), Characterization of the optical properties of atmospheric aerosols in Amazônia from long-term AERONET monitoring (1993–1995 and 1999–2006), *J. Geophys. Res.*, *113*, D04204, doi:10.1029/2007JD009319.

Singh, R. P., S. Dey, S. N. Tripathi, V. Tare, and B. Holben (2004), Variability of aerosol parameters over Kanpur, northern India, *J. Geophys. Res.*, *109*, D23206, doi:10.1029/2004JD004966.

Smirnov, A., B. N. Holben, T. F. Eck, O. Dubovik, and I. Slutsker (2000), Cloud-screening and quality control algorithms for the AERONET database, *Remote Sens. Environ.*, *73*, 337–349, doi:10.1016/S0034-4257(00) 00109-7.

Smirnov, A., B. N. Holben, Y. J. Kaufman, O. Dubovik, T. F. Eck, I. Slutsker, C. Pietras, R. N. Halthore (2002), Optical Properties of Atmospheric Aerosol in Maritime Environments. *J. Atmos. Sci.*, *59*, doi: 10.1175/1520-0469(2002)059<0501:OPOAAI>2.0.CO;2.

Smirnov, A., et al. (2009), Maritime Aerosol Network as a component of Aerosol Robotic Network, *J. Geophys. Res.*, *114*, D06204, doi:10.1029/2008JD011257.

Sokolik, I. N., and O. B. Toon (1999), Incorporation of mineralogical composition into models of the radiative properties of mineral aerosol from UV to IR wavelengths, *J. Geophys. Res.*, 104(D8), 9423–9444, doi:10.1029/1998JD200048.

Tanré, D., Y. J. Kaufman, B. N. Holben, B. Chatenet, A. Karnieli, F. Lavenu, L. Blarel, O. Dubovik, L. A. Remer, and A. Smirnov (2001), Climatology of dust aerosol size distribution and optical properties derived from remotely sensed data in the solar spectrum, *J. Geophys. Res.*, *106*, 18,205–18,217, doi:10.1029/2000JD900663.

Toledano, C., et al. (2011), Optical properties of aerosol mixtures derived from sun-sky radiometry during SAMUM-2, *Tellus*, Ser. B, *63*, 635–648, doi:10.1111/j.1600-0889.2011.00573.x.

Voronoi, G. F. (1908). Nouvelles applications des parametres continus aÂ la theÂorie de forms quadratiques, *J. Reine Agnew. Math.*, *134*, 198-287.

Yang, M., Howell, S. G., Zhuang, J., and Huebert, B. J. (2009), Attribution of aerosol light absorption to black carbon, brown carbon, and dust in China – interpretations of atmospheric measurements during EAST-AIRE, *Atmos. Chem. Phys.*, *9*, doi:10.5194/acp-9-2035-2009.

686 **Table 1.** Previous studies identifying regional aerosol sources affecting AERONET sites

Aerosol Type Source Regions	Affected AERONET Sites	Selected References
Most Regions with Various Types	Most Sites	*Holben et al.* [2001]
Dust - African	Banizoumbou, Capo Verde, Dakar, Ouagadougou, XiangHe, Shirahama	*Tanre et al.* [2001]; *Reid et al.* [2003]
Dust - Asian		*Eck et al.* [2005]
Smoke -Amazonia	Abracos Hill, Alta Floresta	*Eck et al.* [2003b]; *Schafer et al.* [2008]
Smoke - Australian	Lake_Argyle	*Mitchell et al.* [2006]
Smoke - Boreal	Bonanza Creek	*Eck et al.* [2009]
Smoke - African	Mongu	*Eck et al.* [2003a; 2003b]
Pollution - Europe	Ispra	*Melin and Zibordi* [2005]
Mixed - Asia	XiangHe, SEDE_BOKER	*Derimian et al.* [2006]; *Eck et al.* [2010]; *Yang et al.* [2009]
Mixed - India	Kanpur	*Dey et al.* [2004]; *Singh et al.* [2004]; *Prasad et al.* [2007]; *Giles et al.* [2011a]
Mixed - Africa	Ilorin	*Eck et al.* [2010]

687 **Table 2.** Average aerosol absorption and size properties by aerosol type category from AERONET Version 2 almucantar retrievals[a]

Site	Date Range	ω_o 440/675/870/1020 nm	$\alpha_{abs440\text{-}870nm}$	$\alpha_{ext440\text{-}870nm}$	η_{550nm}	N
		Dust				
Banizoumbou	1999-2010	0.91/0.95/0.96/0.96 0.04/0.04/0.04/0.04	1.7±0.6	0.3±0.2	0.28±0.20	2901
Capo_Verde	1999-2010	0.91/0.96/0.97/0.97 0.03/0.03/0.03/0.03	2.0±0.6	0.2±0.2	0.24±0.16	1202
Dakar	2000-2010	0.89/0.95/0.96/0.96 0.03/0.04/0.04/0.03	1.9±0.6	0.3±0.2	0.28±0.23	2250
Ouagadougou	1999-2007	0.90/0.94/0.95/0.95 0.04/0.04/0.04/0.03	1.6±0.5	0.3±0.2	0.30±0.21	1497
Solar_Village	1999-2010	0.91/0.95/0.96/0.96 0.02/0.02/0.02/0.02	1.8±0.6	0.3±0.3	0.28±0.25	3029
		Mixed (for $0.33<\eta_{550nm}\leq 0.66$)				
Ilorin	1999-2009	0.86/0.90/0.92/0.92 0.05/0.05/0.04/0.04	1.6±0.4	0.7±0.2	0.47±0.23	798
Kanpur	2001-2010	0.87/0.90/0.92/0.93 0.03/0.03/0.03/0.03	1.4±0.4	0.7±0.2	0.48±0.22	963
SEDE_BOKER	1999-2010	0.91/0.93/0.93/0.94 0.02/0.02/0.03/0.03	1.2±0.5	0.7±0.2	0.48±0.20	170
XiangHe	2001, 2004-2010	0.88/0.92/0.93/0.93 0.03/0.03/0.03/0.03	1.8±0.4	0.8±0.2	0.53±0.22	446

688 [a] Aerosol optical depth (AOD) at 440 nm is greater than 0.4 for Version 2, Level 2.0 almucantar retrievals. The spectral single
689 scattering albedo (ω_o) averages are listed first followed by their standard deviations. The absorption and extinction Ångström
690 exponents (α_{abs} and α_{ext}) and are computed using the 440-675-870 nm wavelength interval. The fine mode fraction of the AOD
691 (η_{550nm}) is interpolated to 550 nm as discussed in Section 2.

692

693 **Table 2.** (Continued)

Site	Date Range	ω_o 440/675/870/1020 nm	$\alpha_{abs440\text{-}870nm}$	$\alpha_{ext440\text{-}870nm}$	η_{550nm}	N
		Urban/Industrial				
GSFC	1999–2010	0.96/0.95/0.94/0.93 0.02/0.02/0.03/0.03	1.1±0.2	1.8±0.2	0.94±0.20	882
Ispra	1999-2010	0.93/0.93/0.92/0.91 0.03/0.04/0.04/0.04	1.4±0.4	1.6±0.2	0.92±0.24	583
Mexico_City	1999-2010	0.89/0.88/0.86/0.85 0.04/0.04/0.05/0.06	1.3±0.3	1.6±0.2	0.87±0.18	540
Moldova	1999-2010	0.93/0.92/0.90/0.89 0.03/0.04/0.05/0.05	1.2±0.3	1.6±0.3	0.87±0.28	558
Shirahama	2000-2010	0.94/0.93/0.92/0.92 0.03/0.03/0.04/0.05	1.1±0.5	1.3±0.3	0.81±0.35	726
		Biomass Burning				
Abracos_Hill	1999-2005	0.93/0.91/0.90/0.88 0.02/0.03/0.04/0.05	1.3±0.4	2.0±0.1	0.95±0.14	342
Alta_Floresta	1999-2010	0.93/0.92/0.90/0.89 0.02/0.03/0.04/0.05	1.5±0.4	1.9±0.2	0.92±0.18	593
Bonanaza Creek	1999-2005, 2008-2010	0.95/0.96/0.96/0.95 0.03/0.03/0.04/0.04	1.8±0.5	1.5±0.2	0.96±0.22	144
Lake_Argyle	2002-2006, 2009-2010	0.85/0.83/0.82/0.81 0.04/0.05/0.06/0.07	1.4±0.3	1.5±0.4	0.79±0.36	176
Mongu	1999-2007, 2009	0.87/0.83/0.80/0.77 0.03/0.04/0.04/0.05	1.2±0.2	1.9±0.1	0.92±0.10	1411

694

695 **Table 3.** Sensitivity of the absorption Ångström exponent (α_{abs}) to perturbations of single
696 scattering albedo (ω_o) for each dominant aerosol particle type

Type	λ (nm)	α_{abs} [a]	$\delta\omega_o$	$\delta\alpha_{abs}$ [b]			N
		$\delta\omega_o$=0.0		All τ(λ)	τ_{440nm}	τ_{870nm}	
Dust	440-675-870	1.76±0.58	-0.01	-0.27			10879
		1.67±0.52	+0.01[c]	+0.40			9807
		1.76±0.58	-0.02	-0.45			10879
		1.49±0.42	+0.02[c]	+0.67			7290
		1.76±0.58	-0.03[d]	-0.57	+0.47	-0.90	10879
		1.33±0.38	+0.03[cd]	+0.79	-0.54	+1.16	4898
		1.76±0.58	-0.04	-0.67			10879
		1.23±0.36	+0.04[c]	+0.85			3342
Mixed	440-675-870	1.53±0.44	-0.01	-0.09			7199
		1.52±0.42	+0.01[c]	+0.13			7051
		1.53±0.44	-0.02	-0.16			7199
		1.47±0.38	+0.02[c]	+0.23			6623
		1.53±0.44	-0.03[d]	-0.21	+0.40	-0.53	7199
		1.43±0.35	+0.03[cd]	+0.30	-0.51	+0.71	6060
		1.53±0.44	-0.04	-0.25			7199
		1.40±0.33	+0.04[c]	+0.35			5479
Urban/ Industrial	440-675-870	1.21±0.37	-0.01	+0.05			3289
		1.20±0.36	+0.01[c]	-0.10			3174
		1.21±0.37	-0.02	+0.09			3289
		1.19±0.35	+0.02[c]	-0.21			2874
		1.21±0.37	-0.03[d]	+0.12	+0.74	-0.52	3289
		1.18±0.34	+0.03[cd]	-0.31	-1.02	+0.58	2428
		1.21±0.37	-0.04	+0.14			3289
		1.18±0.34	+0.04[c]	-0.40			2027
Biomass Burning	440-675-870	1.35±0.35	-0.01	+0.03			2666
		1.34±0.34	+0.01[c]	-0.04			2639
		1.35±0.35	-0.02	+0.06			2666
		1.33±0.32	+0.02[c]	-0.10			2598
		1.35±0.35	-0.03[d]	+0.08	+0.45	-0.31	2666
		1.32±0.31	+0.03[cd]	-0.19	-0.62	+0.35	2512
		1.35±0.35	-0.04	+0.11			2666
		1.31±0.29	+0.04[c]	-0.29			2421

697 [a] indicates the unperturbed α_{abs} average is recalculated based on available ω_o.
698 [b] indicates wavelength(s) used in perturbation of ω_o.
699 [c] indicates positive perturbation of ω_o must be less than 0.995 for any wavelength.
700 [d] indicates these criteria are the current uncertainty estimates based on *Dubovik et al.* [2000].

701

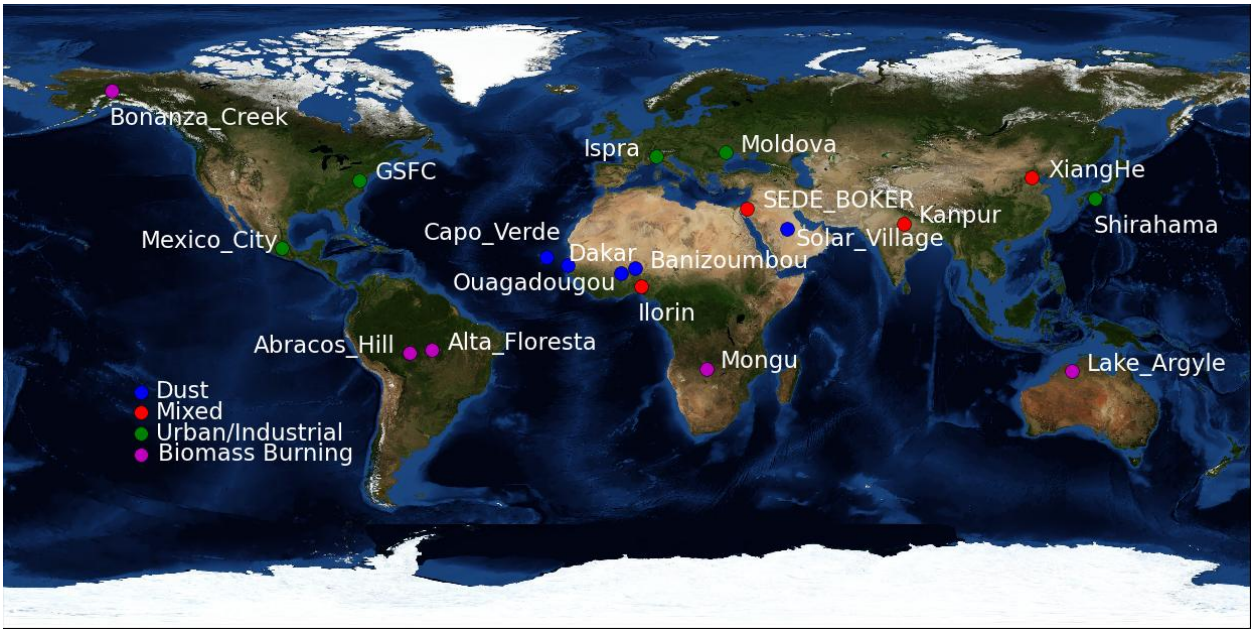

Figure 1. Distribution of the AERONET sites based on the dominant particle type. Sites were selected based on data volume, geographic location, and primary aerosol source region. Other dominant particle types (e.g., sea salt and biogenic aerosols) were not considered due to low aerosol loading conditions ($\tau_{440nm} \leq 0.4$), which was a limiting threshold for AERONET Version 2, Level 2.0 aerosol absorption retrievals [*Dubovik et al*., 2002; *Holben et al*., 2006].

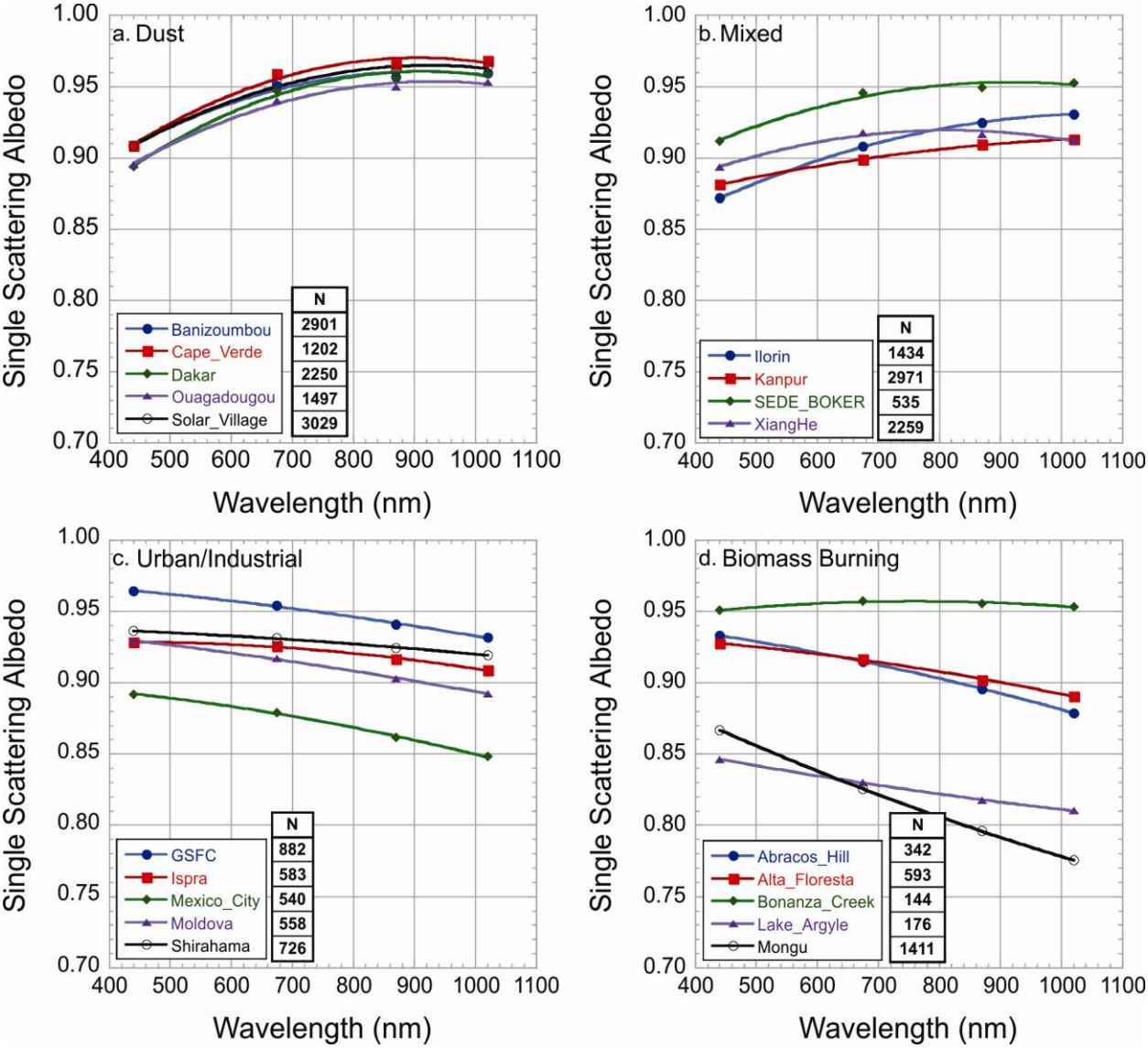

Figure 2. Spectral single scattering albedo averages were grouped by dominant aerosol particle category for τ_{440nm}>0.4 using AERONET Version 2, Level 2.0 data. The plots utilize second order polynomial fit.

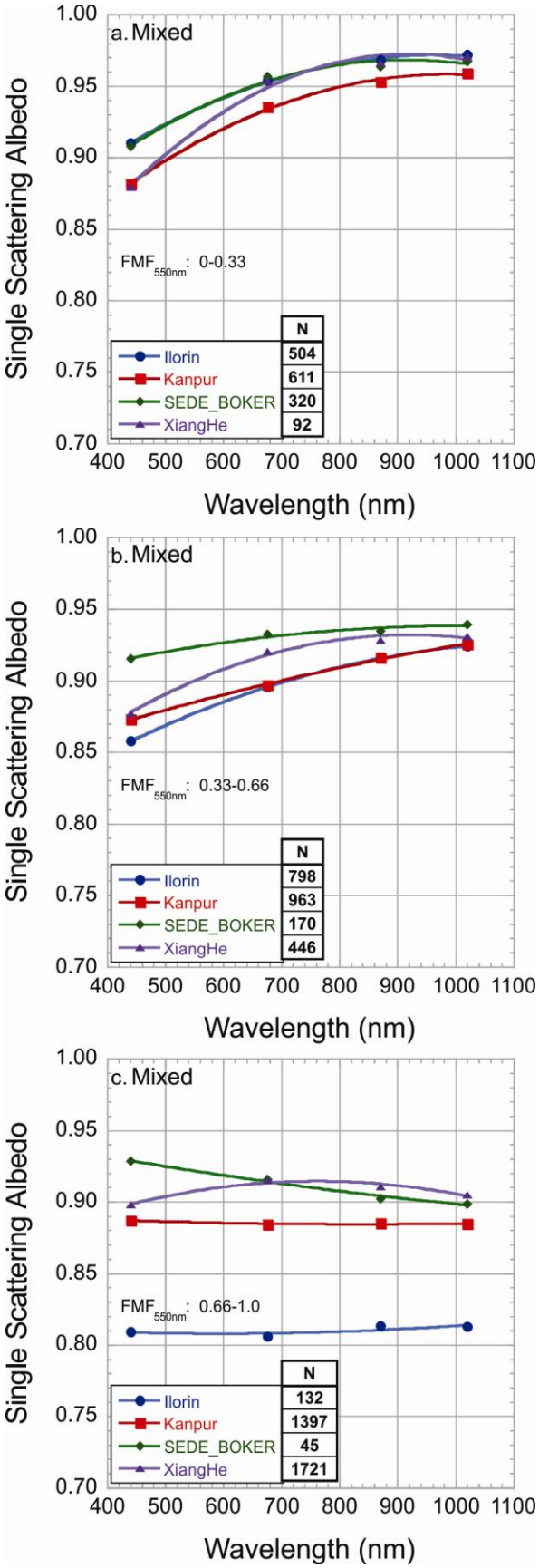

Figure 3. Similar to Figure 2, except the spectral single scattering albedo averages for the Mixed category were grouped by fine mode fraction of AOD (η_{550nm}) using the ranges 0.0-0.33 for coarse mode dominated particles (a), 0.33-0.66 for mixed size particles (b), and 0.66-1.0 for fine mode dominated particles (c).

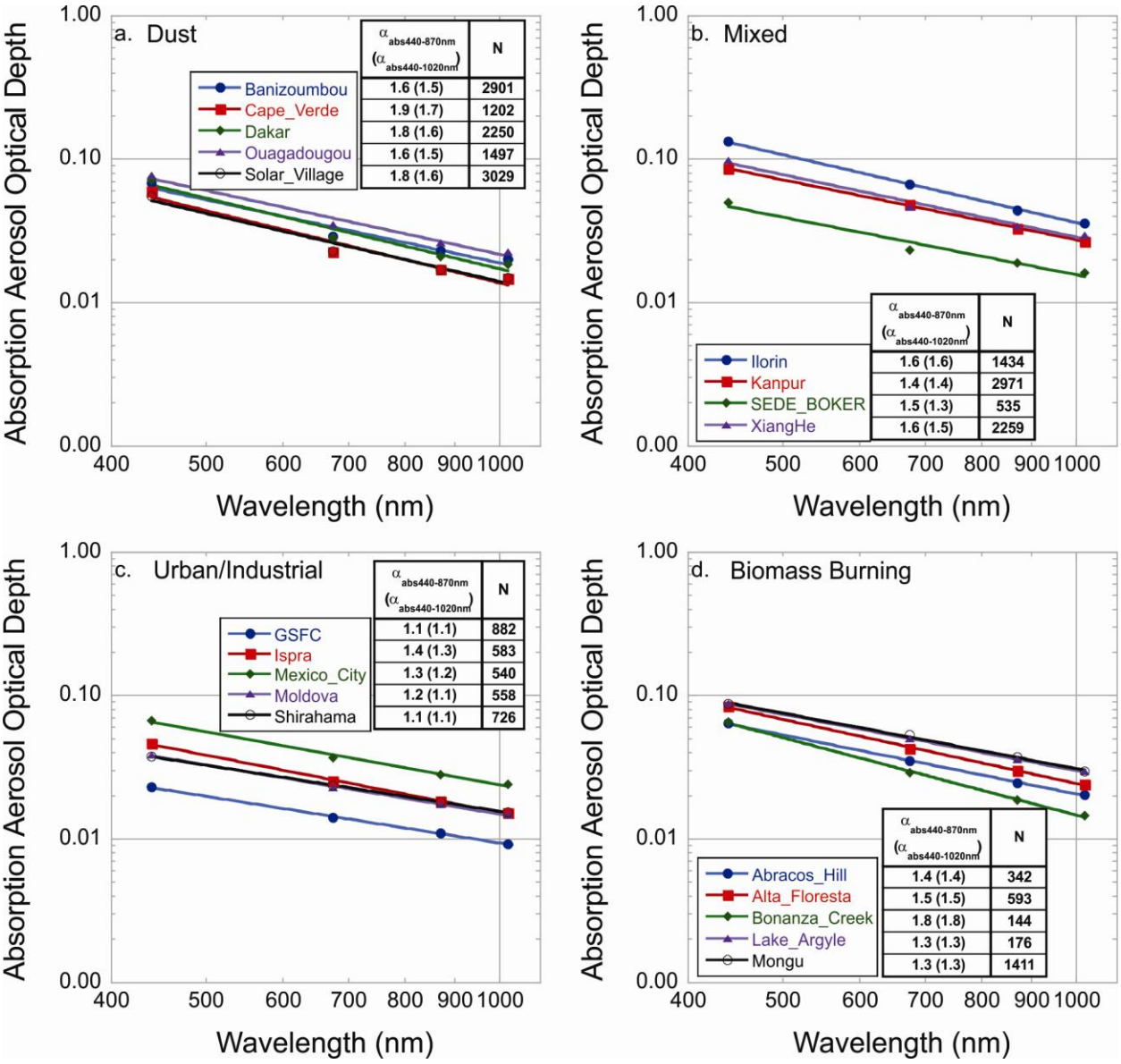

723

724 **Figure 4.** Absorption aerosol optical depth (τ_{abs}) and absorption Ångström exponent (α_{abs})
725 averages were grouped by dominant aerosol particle category for τ_{440nm}>0.4 using AERONET
726 Version 2, Level 2.0 data. The plots use the power law fit and slopes of these lines are the α_{abs}
727 (440-870 nm or 440-1020 nm) listed adjacent to the legend in each plot.

728

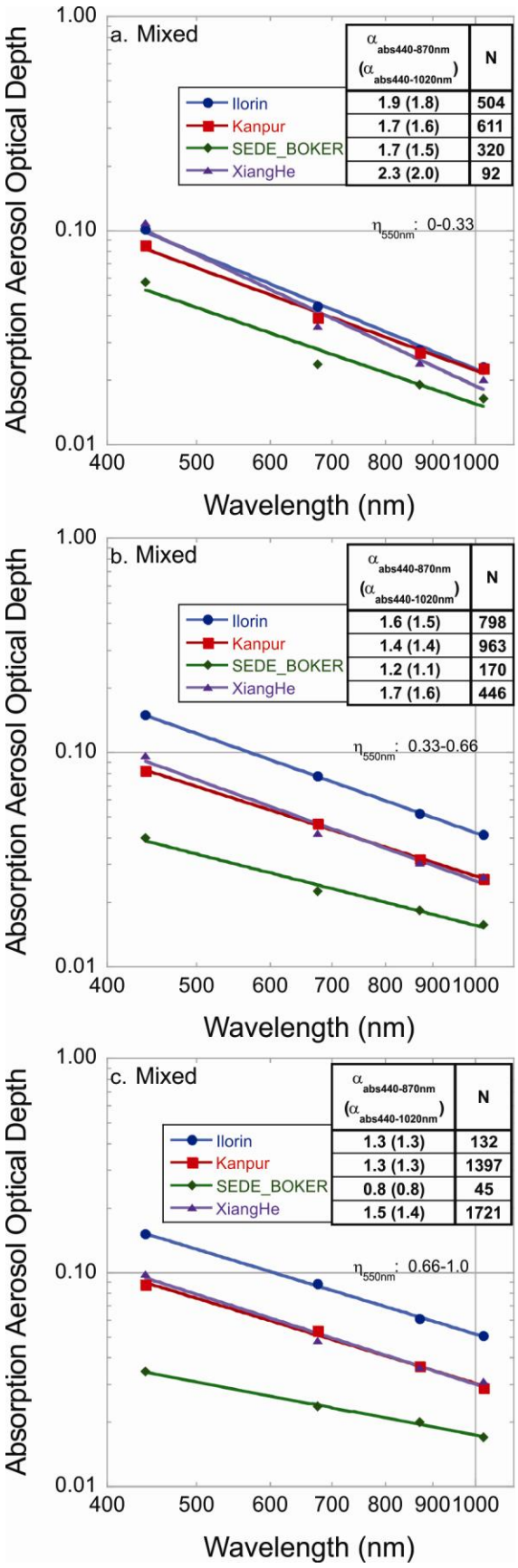

Figure 5. Similar to Figure 3, except τ_{abs} and α_{abs} averages for the Mixed category were grouped by fine mode fraction of the AOD (η_{550nm}) using ranges of 0.0-0.33 for coarse mode dominated particles (a), 0.33-0.66 for mixed size particles (b), and 0.66-1.0 for fine mode particles (c).

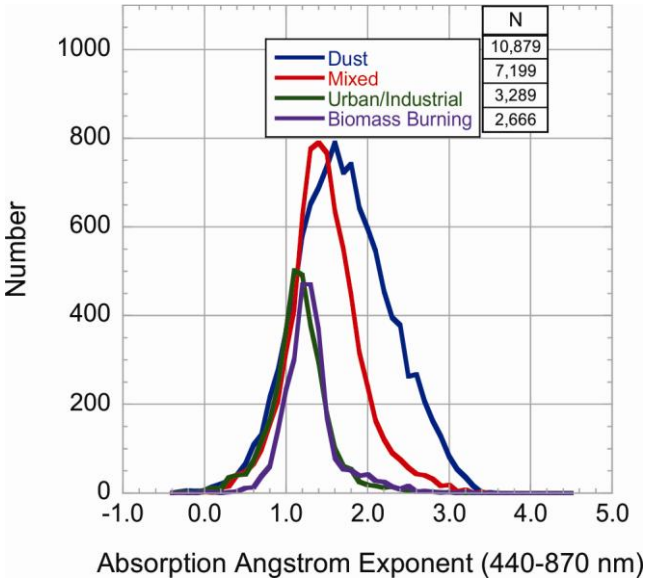

737

738 **Figure 6.** Absorption Ångström exponent (α_{abs}) frequency distribution for each dominant
739 aerosol particle category using AERONET Version 2, Level 2.0 data. Approximately 10% of the
740 α_{abs} retrievals (22% for Urban/Industrial) were below 1.0 or λ^{-1} dependence.

741

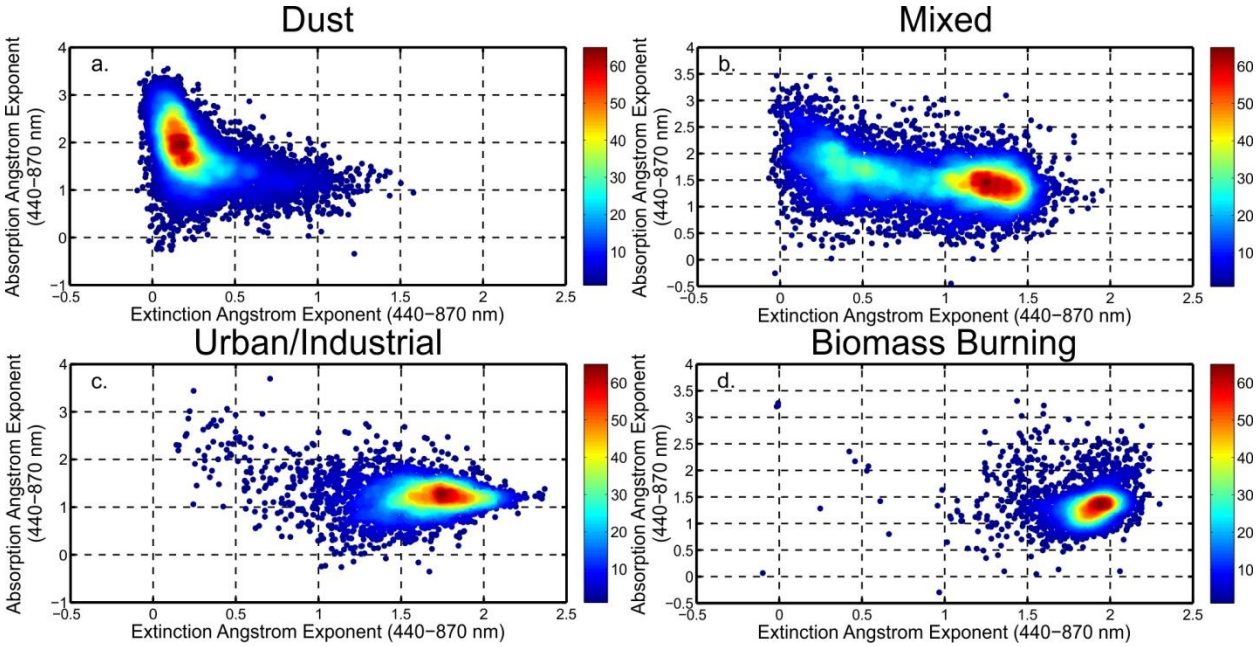

Figure 7. Relative number density plots for the absorption Ångström exponent (440-870 nm) and extinction Ångström exponent (440-870 nm) relationship based on dominant aerosol type using AERONET Version 2, Level 2.0 data. The color scale represents the relative density of points in each aerosol type partitioned data set, where orange to red colors (levels ~45-64) indicate the highest number density based on the Voronoi tessellation.

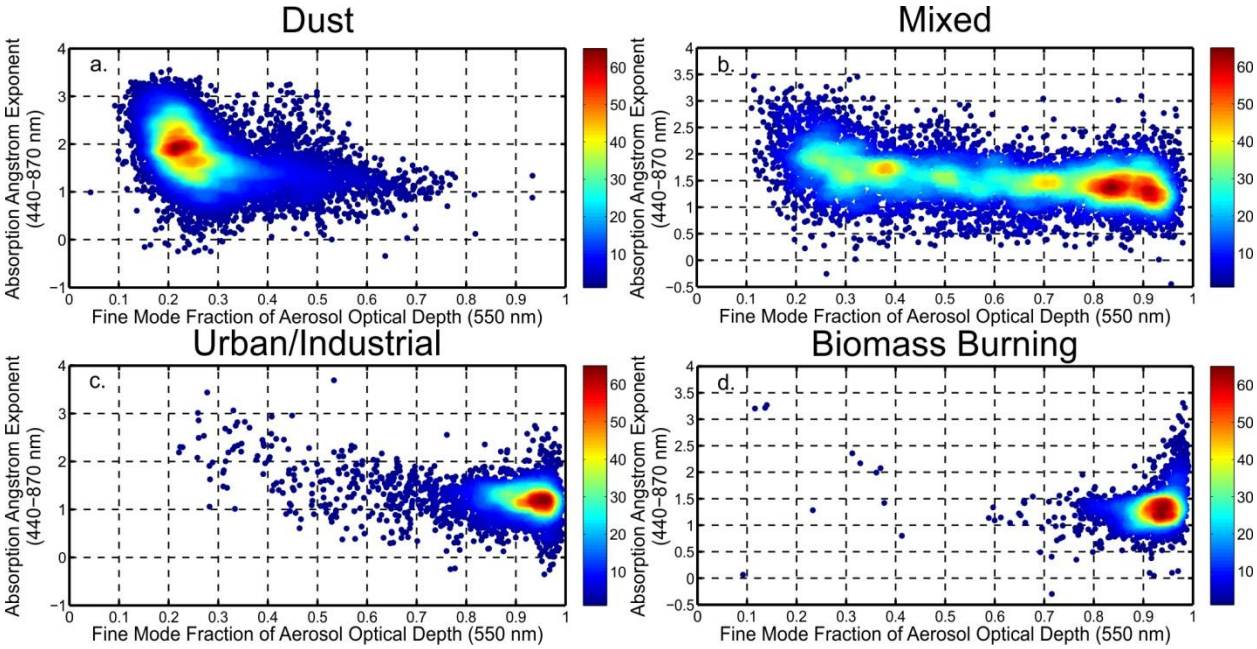

Figure 8. Similar to Figure 7, except for the absorption Ångström exponent (440-870 nm) and fine mode fraction of the aerosol optical depth (550 nm) relationship.

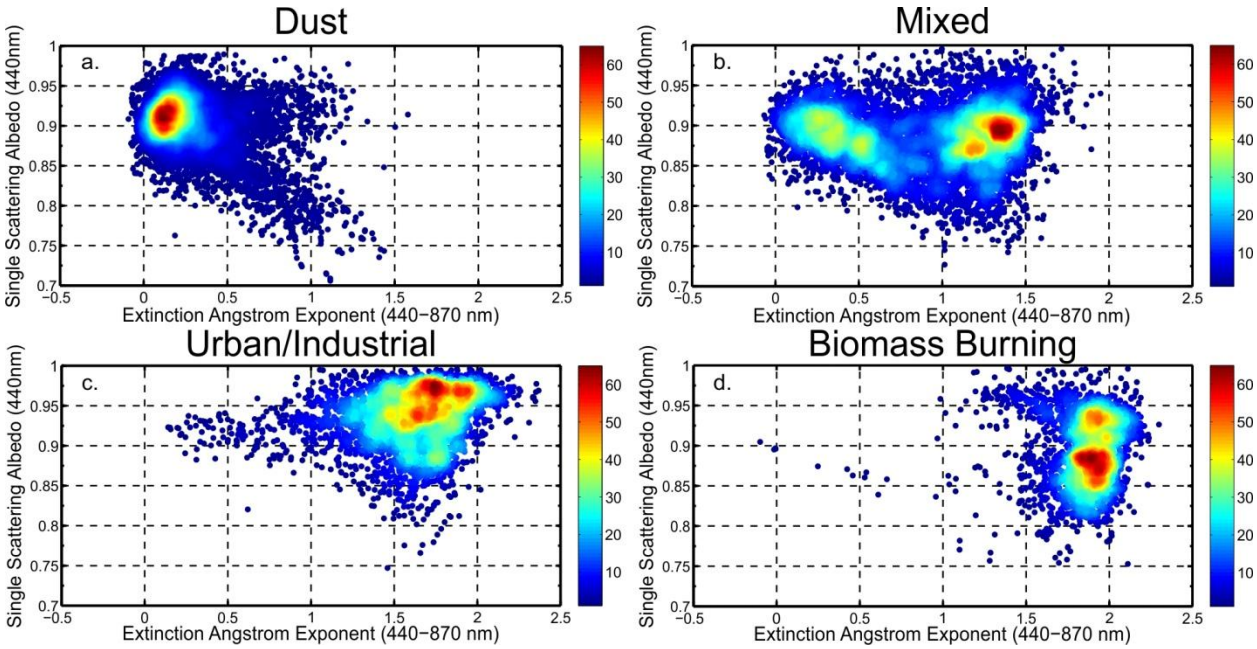

Figure 9. Similar to Figure 7, except for the single scattering albedo (440 nm) and the extinction Ångström exponent (440-870 nm) relationship.

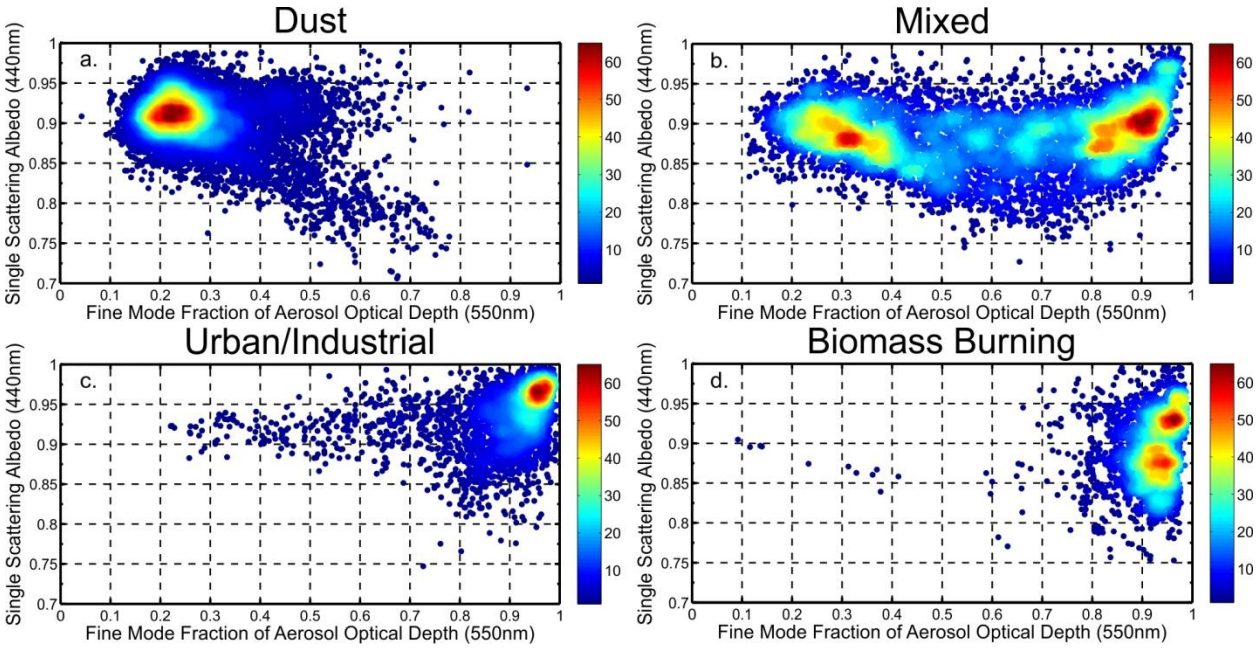

Figure 10. Similar to Figure 7, except for the single scattering albedo (440 nm) and fine mode fraction of the aerosol optical depth (550 nm) relationship.

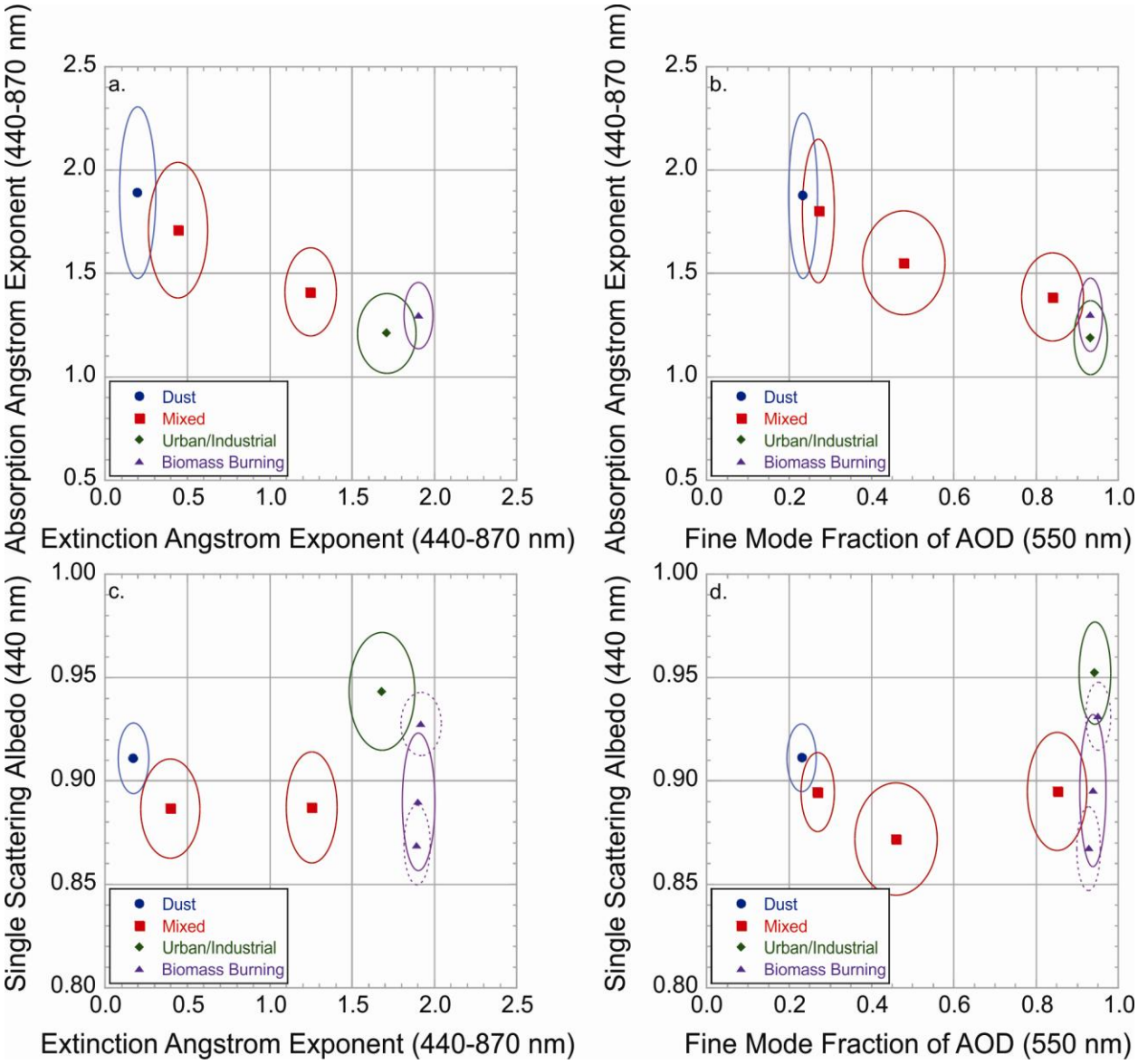

Figure 11. Weighted cluster averages were grouped for each aerosol type category and relationship using AERONET Version 2, Level 2.0 data. The Mixed category averages were calculated using a 0.8 extinction Ångström exponent threshold between mainly small and mainly large particles. For the fine mode fraction of AOD, the Mixed category averages were calculated based on the 0.0-0.33, 0.33-0.66, and 0.66-1.0 ranges. For single scattering albedo plots, the Biomass Burning category was further partitioned by calculating averages using a single scattering albedo threshold of 0.90 to produce two sub-clusters (dashed ellipses) observed in Figure 9 and Figure 10.